Geophysical Journal International

Geophys. J. Int. (2024) **238,** 1723–1741
Advance Access publication 2024 June 21
GJI Geodynamics and Tectonics

https://doi.org/10.1093/gji/ggae217

Intraplate deformation during Gondwana breakup: a study of the Jurassic units of the Cañadón Asfalto Basin (extra-Andean Patagonia, Argentina)

V. Ruiz González [1,2,3] E. M. Renda [4] H. Vizán,[1] F. Martín-Hernández [2,3] A. Palencia-Ortas [5] and M. L. Osete [2,3]

[1] *Instituto de Geociencias Básicas, Aplicadas y Ambientales de Buenos Aires (IGEBA), Universidad de Buenos Aires - CONICET, Intendente Güiraldes* 2160, *Ciudad Autónoma de Buenos Aires C*1428*EHA, Argentina*
[2] *Departamento de Física de La Tierra y Astrofísica, Facultad de Física, Universidad Complutense de Madrid (UCM), Avda. Complutense s/n, Madrid E*-28040, *Spain. E-mail: vruizgonzalez.geologo@gmail.com*
[3] *Instituto de Geociencias IGEO (CSIC-UCM), C/ Dr Severo Ochoa* 7, *Madrid E*-28040, *Spain*
[4] *Instituto de Investigación en Paleobiología y Geología (IIPG), Universidad Nacional de Río Negro - CONICET, Av. Roca* 1242, *General Roca, Río Negro R*8332, *Argentina*
[5] *Departamento de Ingeniería Eléctrica, Electrónica, Automática y Física Aplicada, ETSIDI, Universidad Politécnica de Madrid (UPM), Ronda de Valencia* 3, *Madrid E*-2801, *Spain*

Accepted 2024 June 5. Received 2024 May 27; in original form 2023 June 27

SUMMARY

In this study, we present the results of palaeomagnetic research conducted on Jurassic units of the Cañadón Asfalto Basin (CAB) in Patagonia, formed during Gondwana breakup. This basin is a key locality for understanding intraplate deformation within Patagonia during the Jurassic. The nature of this basin has been a subject of debate, based on the dynamics of the blocks that constitute its depocentres. In this context, the palaeomagnetic study of the Jurassic units of this basin provides a unique methodology to characterize the tectonic motions of its crustal blocks during its formation and development. To achieve this, we collected 350 samples from 53 sites in the sedimentary units of Las Leoneras (ca. 189 Ma) and Cañadón Calcáreo Formations (ca. 160–157 Ma), as well as the volcanic Lonco Trapial Group (ca. 185–172 Ma). The palaeomagnetic results from the sedimentary units show a regional remagnetization due to hydrothermal activity that obliterated the original remanence and overprinted a new one, simultaneously imprinting a secondary remanence in the volcanic units of the Lonco Trapial Group. When comparing the direction of the palaeomagnetic pole obtained from the remagnetized units with respect to average poles of equivalent ages, it is observed that the remagnetization must have occurred during the Late Jurassic (ca. 145 Ma). The age range in which this process occurred (Oxfordian to Aptian) and the direction of the calculated pole dispute a monster polar shift postulated for Late Jurassic to Early Cretaceous times. In addition, the primary magnetization recorded in the units of the Lonco Trapial Group indicates a counterclockwise rotation of the studied crustal blocks between 21° and 11°, which, in line with previous studies, refutes large-scale dextral motion along the Gastre Fault System since the Jurassic. Similar counterclockwise rotations of equivalent magnitudes are found along the units overlying the Palaeozoic Central Patagonian Igneous–Metamorphic Belt, which represents the opposite shear sense compared to the Jurassic units beyond this belt. This is interpreted as a reactivation of the Palaeozoic belt structures in the opposite sense, from transpressive during the Palaeozoic to transtensive during the Mesozoic.

Key words: Palaeomagnetism; Remagnetization; Hydrothermal systems; Continental tectonics: extensional; Intra-plate processes.

1 INTRODUCTION

The Cañadón Asfalto Basin (CAB) was formed during the breakup of Gondwana and spans the southwest and central regions of the North Patagonian Massif in southern South America (Fig. 1a). Its units represent the infills of the rifting stages during Gondwana breakup, coupled with the pre-existing relief of the Palaeozoic basement (e.g. Renda *et al.* 2019; Giacosa 2020) and those created by subsequent inversion tectonics triggered by the Andean Orogeny (e.g. Bilmes *et al.* 2013; Echaurren *et al.* 2016; Allard *et al.* 2021a). The interplay of these three factors contributes to a complex and multifaceted tectonic and structural history of the CAB. In this context, the CAB, given its size and proximity to the southwestern margin of Gondwana, plays a pivotal role in understanding the tectonic evolution of extra-Andean Patagonia during Gondwana breakup (e.g. Homovc *et al.* 1991).

The CAB comprises various depocentres, or sub-basins, separated by basement block highs (Fig. 1b; Homovc *et al.* 1991; Figari *et al.* 1992, 2015; Figari & Courtade 1993), which were formed by asymmetric extensional strain during the Jurassic (e.g. Uliana *et al.* 1989; Figari *et al.* 2015). The controversy about this basin revolves around its formation, either as a pull-apart basin (Silva Nieto *et al.* 2005) or as a basin generated by extension with development of half-grabens, creating the mentioned depocentres, in a basin and range style (Geuna *et al.* 2000; Figari *et al.* 2015). Recent work indicates that the internal structure of the basin does not show evidence of lateral displacement of tectonic blocks due to the lack of subvertical strike-slip faults or flower structures associated with the depocentres in the studied seismic profiles (Allard *et al.* 2021a).

So far, only two palaeomagnetic studies have been conducted on the CAB. Geuna *et al.* (2000) reported that, according to their findings, there was no rotation about vertical axes of tectonic blocks after the Aptian within the study area. Nevertheless, they observed a 25°–30° clockwise rotation in units from the Cañadón Calcáreo Formation (referred to as Upper Cañadón Asfalto Formation in their paper) occurring before that time, specifically between the C and F sampling areas of this study (Fig. 1b). Conversely, further north on the northern flank of the Gastre-Sacanana Fault (45 km to the NE of the E area; refer to Fig. 1b), Zaffarana & Somoza (2012) indicated an anticlockwise rotation about a vertical axis of their studied block since the Early Jurassic, obtained from units of the Lonco Trapial Group (LTG). Additionally, Rapalini & Lopez de Luchi (2000) documented a clockwise rotation at Mamil Choique Range, a basement block of the CAB, obtained from dykes dating to approximately 170 Ma (75 km to the NW of the E area; see Fig. 1). Consequently, a more comprehensive palaeomagnetic study of the Jurassic units in the CAB is essential to clarify potential rotations about vertical axes of the tectonic blocks during the formation of the CAB and to characterize its development since its initiation (Allard *et al.* 2021a).

For this purpose, 52 sites (350 samples) across six areas of the CAB (Fig. 1b) were chosen for sampling and palaeomagnetic study (Fig. 1b). Sampling was carried out in the units of the Jurassic formations Las Leoneras (Nakayama 1973), Cañadón Calcáreo (Proserpio 1987; Cúneo *et al.* 2013) and the LTG (Lesta & Ferello 1972; Fig. 1c).

1.2 Geological background

1.2.1 Lithostratigraphic units

The infill of the CAB overlies Palaeozoic and Triassic units (Dalla Salda *et al.* 1991, 1994). The oldest unit within the CAB is the Las Leoneras Formation (Nakayama 1973) which yielded a zircon U-Pb age of 188.949 ± 0.096 Ma at the top of the unit in its type locality (Cúneo *et al.* 2013). The Las Leoneras Formation overlies Palaeozoic granitoids and consists of fluvial/alluvial and lacustrine deposits, including conglomerates, sandstones, mudstones, limestones and tuffs. This formation represents the initial stage of passive rifting and serves as the first unit of the J_1 megasequence proposed by Figari *et al.* (2015).

The volcaniclastic LTG (Lesta & Ferello 1972) is mainly composed of lavas which often exhibit autobrecciation, as well as gravitational flows of blocks, ash, lahar and ignimbrites. Within the area of this study, it presents alternations of sedimentary deposits at the base and top of the Group, showing transitional contacts with the Las Leoneras Formation (Di Capua & Scasso 2020) and the Cañadón Asfalto Formation (Figari *et al.* 2015), respectively. Likewise, beyond the studied area, this group overlies Palaeozoic units and the Central Patagonian Batholith (e.g. Zaffarana & Somoza 2012). The units of this group also present lateral changes of volcanogenic lithofacies close to volcanic edifices, indicating the alternation of explosive and effusive events (Figari *et al.* 2015). Several radiometric ages have been determined for this group (data obtained with K-Ar dating method have been discarded in this work): 185.39 ± 0.99, 184 ± 5, 182.8 ± 1.3 and 178.9 ± 1.1 Ma (amphibole Ar-Ar ages, Zaffarana & Somoza 2012; Zaffarana *et al.* 2018), and 172.3 ± 1.8 Ma (zircon U-Pb age, Hauser *et al.* 2017). These units, part of the J_1 megasequence, exhibit minor unconformities, representing the development of half-grabens during the rifting of the CAB (Figari *et al.* 2015). Also, several epithermal deposits have been described in this formation, like the Santa Máxima polymetallic deposit (e.g. Sangster 2001; Fernández *et al.* 2008; see Fig. 1).

The overlying formation, known as the Cañadón Asfalto Formation (Stipanicic *et al.* 1968), is characterized by the infills of the contemporaneously forming half-grabens. This formation comprises basalts alternating with lacustrine carbonate levels and black mudstones in the lower member. It is overlain by the lacustrine sedimentary successions of the upper member of the formation (Allard *et al.* 2021a). Several radiometric ages have been obtained from this formation: 182.8 ± 0.8 Ma (sanidine Ar-Ar age, Márquez *et al.* 2016), 179.481 ± 0.059, 179.41 ± 0.13, 178.766 ± 0.092, 177.37 ± 0.12, 177.27 ± 0.40, 176.6 ± 6.4, 176.15 ± 0.12, 173.9 ± 1.9, 173.6 ± 6.4, 170.8 ± 3.0 and 168.2 ± 2.2 Ma (zircon U-Pb ages, Cúneo *et al.* 2013; Bouhier *et al.* 2017; Hauser *et al.* 2017; Fantasia *et al.* 2021). This formation marks the final unit of the J_1 megasequence (Figari *et al.* 2015). Also, it is characterized by the presence of epithermal deposits, as the Navidad world-class Ag + Pb district (Márquez *et al.* 2016; Bouhier *et al.* 2017; see Fig. 1).

The Cañadón Calcáreo Formation disconformably overlays the preceding formations and is characterized by the absence of carbonate rocks (Proserpio 1987). In this study, this formation is identified following the criteria of Cúneo *et al.* (2013) and Figari *et al.* (2015). The age of this formation has been determined through several radiometric ages: 160.3 ± 1.7, 158.3 ± 1.3, 157.449 ± 0.056 and 157.387 ± 0.045 Ma (zircon U-Pb ages; Cúneo *et al.* 2013; Hauser *et al.* 2017). The 147.1 ± 3.3 Ma biotite K-Ar age by Cabaleri *et al.* (2010) has been discarded. It comprises reddish sandstones, conglomerates, mudstones and some pyroclastic deposits, which exhibit significant lateral variations in lithofacies and thicknesses (Proserpio 1987; Figari *et al.* 2015; Allard *et al.* 2021b). This unit represents the J_2 megasequence, indicating the infill of mature half-grabens and the conclusion of the rifting process (Figari *et al.* 2015). In addition, this formation also presents barite mineralization zones linked to hydrothermal activity (Fernández Lima & Latorre 1978).

The Albian Chubut Group overlies the Jurassic succession through an angular unconformity (Lesta 1968; Navarro *et al.* 2015;

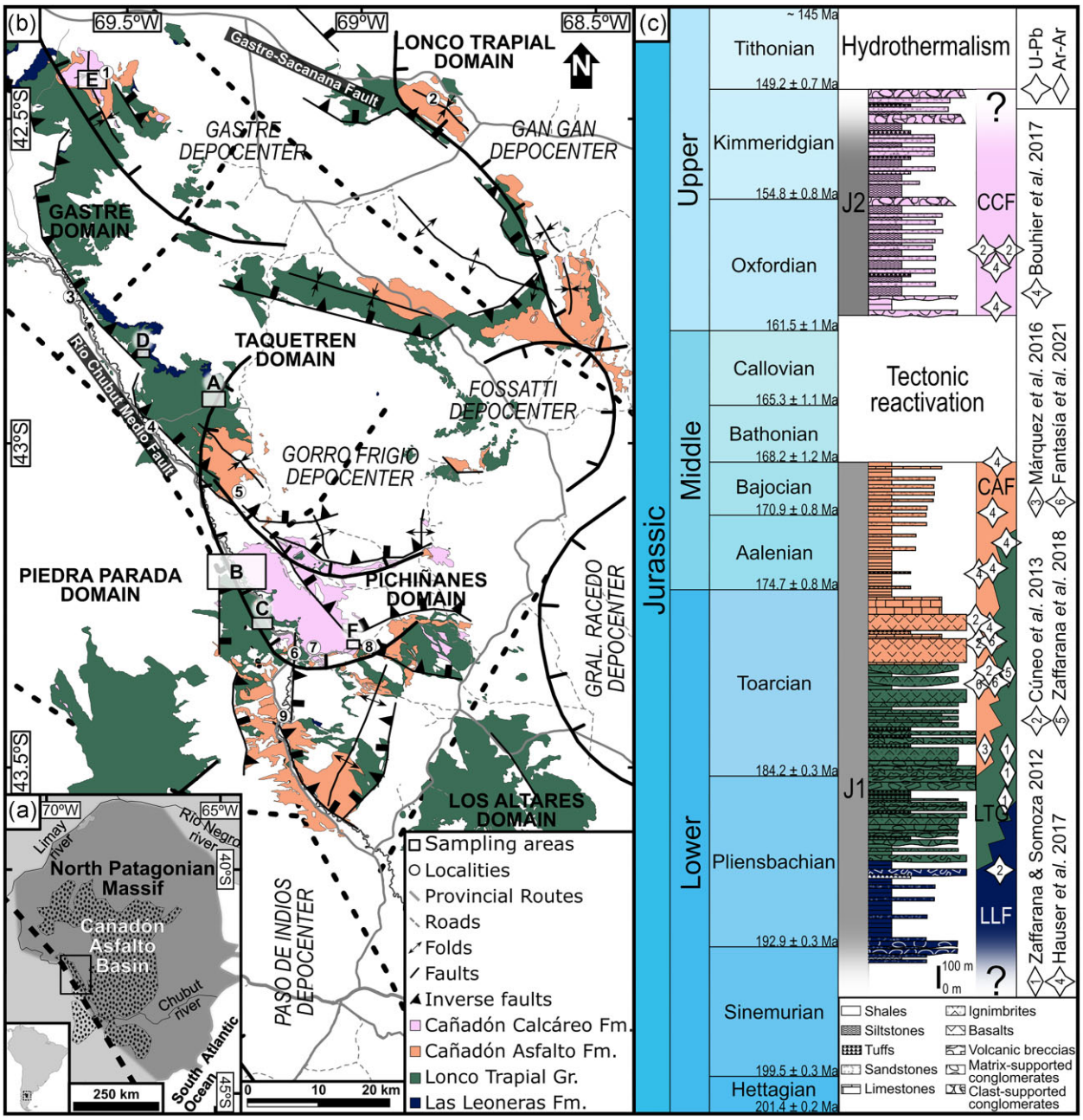

Figure 1. (a) Regional map of the North Patagonian Massif where the CAB is indicated with a dotted pattern (modified from Figari *et al.* 2015) and the study area of this work is highlighted with a square. The Palaeozoic suture between northern and southern Patagonia proposed by Renda *et al.* (2019) is marked with a discontinuous bold line. (b) Map of the studied area (modified from Bilmes *et al.* 2013; Cúneo *et al.* 2013; Figari *et al.* 2015; Allard *et al.* 2021a; Ardolino *et al.* 2022). The sampling areas in this work presented in Fig. 2 are highlighted with squares. Also, the localities mentioned in the text are marked with numbers: (1) Yanquetruz post, (2) Navidad District, (3) Paso del Sapo, (4) Evaristo Fernandez bridge, (5) Gorro Frigio Peak, (6) El Torito ranch, (7) Santa Máxima Canyon, (8) El Quemado post and (9) Cerro Cóndor. The basement blocks determined by Renda *et al.* (2019) are delimited with a discontinuous bold line. Non-Jurassic units have been omitted. (c) Stratigraphic column with the Jurassic chronostratigraphic column (left; Cohen *et al.* 2013, updated), the Jurassic megasequences (J_1 and J_2) and tectonic stages (centre; modified from Figari *et al.* 2015), and the stratigraphic units with the U-Pb and Ar-Ar datings (right): Cañadón Calcáreo Formation (CCF), Cañadón Asfalto Formation (CAF), Lonco Trapial Group (LTG) and Las Leoneras Formation (LLF).

Butler *et al.* 2020). Above these units, the Maastrichtian–Danian marine formations Paso del Sapo and Lefipán are found in subtle unconformity (Lesta & Ferello 1972). Together, these formations constitute the K megasequence, which represents the post-rift stage of the CAB triggered by regional thermal subsidence (Figari *et al.* 2015).

During Cenozoic, reactivation of normal faults as reverse faults due to inversion tectonics led to the generation of new sub-basins. An example is the case of the Gastre Basin (e.g. Bilmes *et al.* 2013; Bucher *et al.* 2019). These continental basins are interspersed with Eocene basic volcanic eruptions (Mazzoni *et al.* 1991).

1.2.2 Structural features

From a regional point of view, the area is characterized by two dominant sets of structural lineaments: the 'Gastre System' oriented in an NW-SE direction, and the 'Comallo System' oriented in an NNW-SSE (Coira *et al.* 1975), which are associated with parallel and conjugate faults (e.g. Dalla Salda & Franzese 1987; Giacosa 2020). These fractures and faults, inherited from Palaeozoic times, are pervasive throughout the entire study area and SW of the North Patagonian Massif (e.g. Renda *et al.* 2019; see Figs 1a and b), and present local senses of shear prior to the formation of the CAB (e.g. Zaffarana *et al.* 2010, 2012, 2017). Two prominent structures align with these lineament trends in the study region: the NW-SE Gastre-Sacanana Fault and the NNW-SSE Río Chubut Medio Fault (Bilmes *et al.* 2013; see Fig. 1b). These structures experienced intense Cenozoic reactivation (Savignano *et al.* 2016), generating the inversion of many faults and cutting some lineaments due to the W-E compression of the Andean Orogeny that exhumed the edges of the Taquetrén and Jalalaubat mountain ranges, among others (Figari & Courtade 1993; Ruiz González *et al.* 2020).

Therefore, Palaeozoic structures play a crucial role in shaping and controlling the development and infill of the sub-basins or depocentres within the CAB (Fig. 1b). In this regard, Renda *et al.* (2019) propose a group of basement blocks correlating geophysical data and structural elements (see Fig. 1b). This structure of Palaeozoic blocks spreads from the CAB to the San Jorge Gulf Basin, which implies compartmentalization of the Cañadón Asfalto and San Jorge Gulf basins since the beginning of the pre-rift stage (Foix *et al.* 2020).

The depositional record within the CAB sub-basins provides essential insights into the deformational episodes, or megasequences, involving different sets of structures and strain orientations (Figari *et al.* 2015). In this sense, several structural studies have been conducted in the north part of the North Patagonian Massif (Benedini & Gregori 2013; Benedini *et al.* 2014, 2021; González *et al.* 2014, 2016; Barros *et al.* 2020). One of the most recent proposes that four different strain partitions developed during the Lower to Middle Jurassic, where the last two were contemporaneous with the CAB formation: (1) the Lower Pliensbachian–Toarcian NNW-oriented transpressive phase, and (2) the Callovian–Bajocian NE contractional phase (Benedini *et al.* 2022). In this work, they relate the reactivation of W-E to WNW-ESE-oriented regional transfer zones with the Lower Pliensbachian to Toarcian stress partition of the northern Patagonia, which are predominantly constituted by dextral strike-slip faults.

2 METHODS

2.1 Sampling characteristics

Palaeomagnetic samples were collected using a hand-drilling machine and oriented with magnetic and sun compasses. In certain cases, multiple specimens were obtained from longer cores. The sampling of the LTG (I), Las Leoneras Formation (II) and Cañadón Calcáreo Formation (III) was conducted in six distinct areas, as depicted in Figs 1(b) and 2. These areas correspond to three specific basement blocks identified by Renda *et al.* (2019): the E area within the Gastre domain, the A and D areas within the Taquetren domain, and the B, C and F areas within the Pichiñanes domain (refer to Fig. 1b).

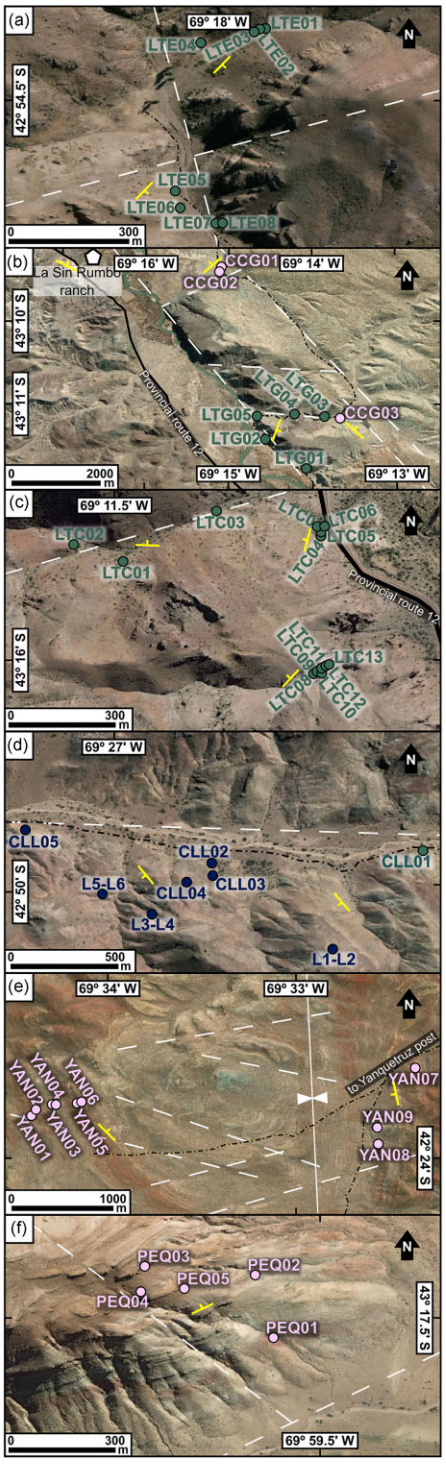

Figure 2. Aerial view of the sampled sites within the different areas along the Chubut River and its surroundings: (a) LTG in the Evaristo Fernández Canyon; (b) LTG and Cañadón Calcáreo Formation to the south of the Gorro Frigio peak; (c) LTG at 7 km to the NW of the El Torito ranch; (d) Las Leoneras Formation in the eponymous canyon; (e) Cañadón Calcáreo Formation in the anticline to the SW of the Yanquetruz post and (f) Cañadón Calcáreo Formation in the eponymous canyon, to the west of El Quemado post. The location of these areas is also highlighted in Fig. 1(b). Inferred faults are marked with dashed lines, and the fold of the Yanquetruz post area with a solid line. The bedding planes of the units are indicated with perpendicular lines (see Tables 1 and 2). Roads are marked with dashed lines and routes with solid lines.

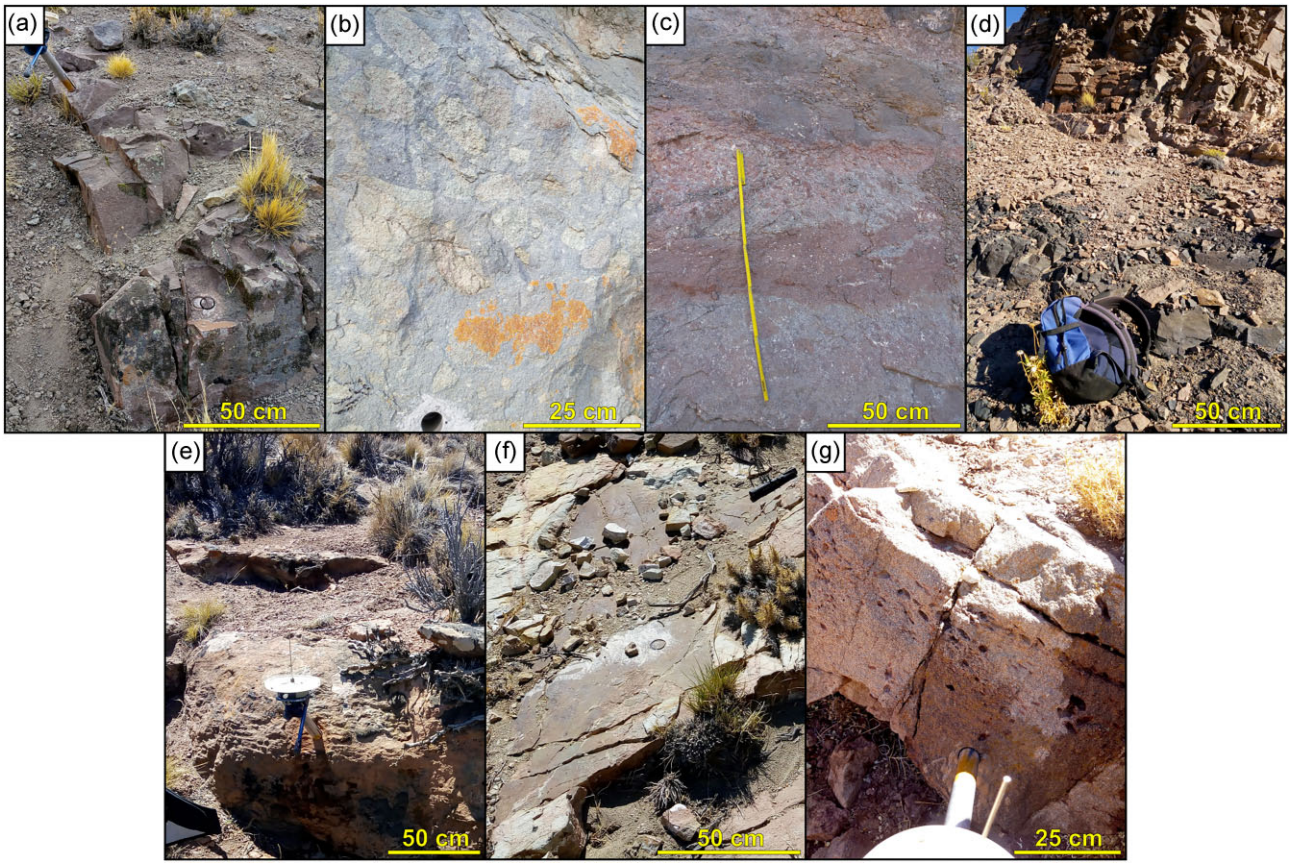

Figure 3. Representative sampled units of the CAB: (a) andesitic lavas of the LTG in the A area (LTE04), (b) pumice clast-rich ignimbrite of the LTG in the B area (LTG02); (c) intercalation between scoria and auto-brecciated lavas and lavas of the LTG in the C area (LTC13); (d) sandstones and mudstones of the Las Leoneras Formation in the D area (CLL05); (e) sandstones of the Cañadón Calcáreo Formation in the E area (YAN02),(f) tuffaceous sandstone of the Cañadón Calcáreo formation in the B area (CCG01) and (g) coarse sandstones of the Cañadón Calcáreo Formation in the F area (PEQ05).

I. The LTG was sampled in three areas, showing different lithological associations (Figs 2a–c):

(a) The Evaristo Fernández Canyon was the first sampling area (A area, LTE sites), located 12 km ENE of the eponymous bridge (see Figs 1b and 2a). There, the units comprise brown-reddish and grey-purplish andesitic lavas, pyroclastic deposits with grey to violet colours, and coarse-grained and yellow-greenish lahar-type deposits (Fig. 3a). From this area, 55 samples were obtained from eight sites (Table 1).

(b) The second area where the LTG was sampled is located 15 km south of the Gorro Frigio Peak (B area, LTG sites), at the eastern margin of the Chubut River (see Figs 1b and 2b). The outcrops from this area are ignimbrites and pyroclastic deposits, where the main surges transport decimetric to metric pumice clasts (Fig. 3b). Five sites were drilled, obtaining 43 samples (Table 1).

(c) The last sampled outcrops of the LTG are located at the western margin of the Chubut River, 7 km NW of the El Torito Ranch (C area, LTC sites; see Figs 1b and 2c). These units are part of a volcanic cinder cone, which comprises intercalations between scoria and ash deposits, as well as juvenile bombs that are deformed along bedding inclination, and lavas or autobrecciated lavas (Fig. 3c). From a total of 13 sites 89 samples were obtained, collecting between six and ten samples per site (Table 1).

II. The samples collected from the Las Leoneras Formation were obtained in the Las Leoneras Canyon (D area, CLL and L sites), located at the eastern margin of the Chubut River (Figs 1b and 2d). This sampling was carried out following the stratigraphic section cropping out in this canyon, sampling greyish to brownish fine-grained sedimentary units with different degrees of recrystallization (Di Capua & Scasso 2020; Fig. 3d). Nine sites were sampled, obtaining a total of 54 samples, from which one corresponds to a brown-greenish sill assigned to the LTG (CLL01 site from the Fig. 2d). Because of the fragility of the rocks only a single specimen was obtained from each sample (Table 2).

III. The Cañadón Calcáreo Formation was sampled in three areas (Fig. 1b):

(a) West of the Yanquetruz Post (E area, YAN sites; Fig. 2e), six and three sites from the west and the east flanks of a synclinal fold were sampled, respectively (Fig. 2e). These sampled units are mustard to khaki and dark purple mudstones, and reddish coarse to fine-grained sandstones (Fig. 3e). In this area also recrystallized fracture zones linked to hydrothermal activity can be recognized. To avoid possible remagnetizations linked to these fractures, those zones were avoided in the sampling. A total of 56 samples were obtained from nine sites (Table 2).

(b) In the southern region of the Gorro Frigio Peak (B area, CCG sites; Fig. 2b), the Cañadón Calcáreo Formation was sampled at the eastern margin of the Chubut River, where it overlies the units of the LTG. Two sampling sites were located in yellow-coloured tuffs and fine-grained sandstones with bivalves (CCG01 and CCG02, Fig. 3f). Additionally, a third site (CCG03) was sampled further

Table 1. Geographic coordinates of the LTG sampled sites and the statistical parameters (Fisher 1953) of the obtained M component directions. *n*/*N* = used samples/total samples.

Sampling area	Lithology	Site	Site coordinates		*n*/*N*	Geographic coordinates					Bedding	Stratigraphic coordinates					VGP (TILT)	
			Lat. (°S)	Long. (°W)		Dec.	Inc.	*R*	*k*	α95	(strike/dip)	Dec.	Inc.	*R*	*k*	α95	Lat. (°S)	Long. (°E)
A	Lava	LTE01	42.9067	69.2990	3/5	360.0	−46.1	3.0	59.1	16.2	44/20	349.5	−30.8	3.0	58.6	16.2	62.2	88.8
	Lava	LTE02	42.9067	69.2991	5/6	348.3	−69.5	5.0	132.4	6.7	44/20	332.4	−51.4	5.0	132.6	6.7	65.7	38.0
	Dyke	LTE03	42.9068	69.2992	5/11	354.1	−80.8	4.9	27.2	14.9	44/20	326.8	−62.4	4.9	27.3	14.9	66.0	7.4
	Ignimbrite	LTE05	42.9103	69.3009	6/6	208.1	62.4	5.9	81.0	7.5	44/20	180.5	52.1	5.9	80.9	7.5	79.8	113.0
	Ignimbrite	LTE06	42.9103	69.3009	6/6	206.1	69.7	6.0	368.8	3.5	44/20	172.1	57.6	6.0	369.4	3.5	82.4	55.8
	lahar	LTE08	42.9110	69.2999	5/5	268.4	74.1	4.9	59.2	10.0	44/20	186.7	75.8	4.9	59.2	10.0	69.4	282.0
B	Ignimbrite	LTG01	43.1967	69.2346	6/12	357.6	−56.1	5.8	22.7	14.4	20/15	340.8	−48.3	5.8	22.7	14.4	69.3	56.6
		LTG02	43.1905	69.2428	3/3	195.8	28.8	2.9	21.0	27.6	20/15	187.9	26.7	2.9	21.0	27.6	60.1	126.3
		LTG03	43.1859	69.2309	5/6	6.2	−53.9	4.9	65.3	9.5	20/15	348.9	−48.1	4.9	65.6	9.5	73.4	74.7
		LTG04	43.1854	69.2369	3/4	358.9	−55.1	3.0	108.1	11.9	20/15	342.4	−47.6	3.0	107.4	12.0	69.8	60.6
		LTG05	43.1864	69.2445	5/6	201.6	38.6	4.9	46.9	11.3	20/15	189.8	37.4	4.9	46.9	11.3	66.3	134.1
A + B				Mean normal	6/11	358.9	−60.3	5.9	39.8	10.7		341.4	−48.4	5.9	48.7	9.7		
				Mean reverse	5/11	207.0	56.5	4.7	12.1	23.0		184.1	50.1	4.8	17.6	18.7		
				Total mean	11/11	12.1	−59.4	10.5	18.3	11.0		351.3	−49.7	10.6	23.9	9.5		
	Positive reversal test			Classification C			$\gamma_c =$	18.1	$\gamma_o =$	14.9								
C																		(GEO)
	Lava	LTC01	43.2641	69.1914	8/8	27.7	−44.5	7.9	97.3	5.6	272/27	52.6	−66.4	7.9	96.8	5.7	61.8	172.6
		LTC02	43.2637	69.1927	7/7	24.0	−55.4	7.0	195.6	4.3	272/27	67.9	−76.5	7.0	196.4	4.3	70.2	187.3
		LTC03	43.2629	69.1891	5/5	11.1	−58.0	5.0	209.9	5.3	272/27	48.1	−83.4	5.0	210.8	5.3	80.5	175.9
		LTC04	43.2635	69.1865	7/7	145.0	85.2	6.9	74.4	7.0	205/19	285.7	75.0	6.9	74.1	7.1	50.8	299.5
		LTC05	43.2634	69.1865	8/8	152.8	83.1	7.9	87.4	6.0	205/19	277.4	75.8	7.9	87.3	6.0	54.9	301.6
		LTC06	43.2633	69.1864	4/5	123.9	79.4	4.0	66.7	11.3	205/19	284.3	81.3	4.0	66.7	11.3	51.6	318.7
		LTC07	43.2633	69.1865	5/6	223.5	82.8	5.0	104.0	7.5	205/19	276.8	67.7	5.0	103.7	7.5	52.5	274.8
		LTC08	43.2670	69.1866	7/7	180.7	75.9	6.9	103.7	6.0	190/26	248.3	62.7	6.9	103.1	6.0	70.0	289.8
		LTC09	43.2670	69.1866	6/6	154.7	79.9	6.0	174.8	5.1	190/26	257.1	68.3	6.0	174.6	5.1	39.6	238.9
		LTC10	43.2670	69.1865	6/6	195.4	73.7	6.0	245.0	4.3	226/33	285.0	62.0	6.0	246.2	4.3	71.1	263.5
		LTC11	43.2670	69.1865	7/7	202.6	71.0	7.0	249.4	3.8	226/33	279.6	60.3	7.0	255.0	3.8	71.0	248.6
		LTC12	43.2668	69.1864	5/6	185.8	72.7	5.0	135.8	6.6	219/28	269.8	66.8	5.0	136.2	6.6	74.7	279.0
		LTC13	43.2668	69.1864	7/7	213.2	74.6	7.0	153.8	4.9	255/20	294.6	75.1	7.0	154.2	4.9	63.4	254.7
				Mean normal	3/13	21.7	−52.8	3.0	84.3	13.5		56.7	−75.6	3.0	83.6	13.6		
				Mean reverse	10/13	184.1	79.2	9.9	112.2	4.6		274.1	70.0	9.9	87.6	5.2		

Table 2. Geographic coordinates of the sampled units of the Las Leoneras and Cañadón Calcáreo formation and the statistical parameters (Fisher 1953) of the obtained M component remanence directions. *n*/*N* = used samples/total samples. Discarded sites because of their anomalous position are highlighted in grey.

Sampling area	Lithology	Site	Site coordinates		*n*/*N*	Geographic coordinates					VGP (GEO)		Bedding	Stratigraphic coordinates				
			Lat. (°S)	Long. (°W)		Dec.	Inc.	*R*	*k*	α95	Lat. (°S)	Long. (°E)	(strike/dip)	Dec.	Inc.	*R*	*k*	α95
D	Sandstone	CLL02	42.8322	69.4459	6/6	1.1	−56.3	6.0	138.8	5.7	84.0	119.1	140/25	18.5	−36.8	6.0	139.3	5.7
	Mudstone	CLL03	42.8322	69.4459	3/3	12.7	−58.5	3.0	63.2	15.6	79.8	184.5	140/25	26.8	−36.7	3.0	62.9	15.7
	Mudstone	CLL04	42.8331	69.4470	6/6	2.8	−56.0	5.9	61.7	8.6	83.4	130.6	140/25	19.5	−36.2	5.9	61.9	8.6
	Sandstone	CLL05	42.8308	69.4537	3/3	7.2	−63.6	2.9	23.3	26.1	84.3	227.3	140/25	25.9	−42.3	2.9	23.4	26.1
	Mudstone	L3-L4	42.8351	69.4483	4/5	337.1	−57.4	4.0	152.8	7.5	72.0	28.5	140/25	4.1	−44.1	4.0	151.6	7.5
				Mean values	5/5	360.0	−58.9	5.0	108.8	7.4				19.2	−39.5	5.0	108.4	7.4
E	Sandstone	YAN01	42.3964	69.5735	6/6	346.7	−51.2	6.0	148.0	5.5	75.1	60.9	315/16	325.8	−57.2	6.0	148.6	5.5
	Sandstone	YAN02	42.3958	69.5731	5/6	357.2	−54.0	4.9	35.1	13.1	81.8	93.7	315/16	334.7	−62.4	4.9	34.9	13.1
	Mudstone	YAN04	42.3954	69.5714	5/6	3.2	−59.1	5.0	126.4	6.8	86.5	155.1	315/16	335.9	−68.5	5.0	126.6	6.8
	Mudstone	YAN05	42.3953	69.5695	6/6	348.2	−50.5	5.9	53.5	9.2	75.4	66.3	315/16	327.9	−56.9	5.9	53.6	9.2
	Sandstone	YAN06	42.3952	69.5691	5/5	338.5	−46.1	4.9	57.7	10.2	67.0	54.1	315/16	321.0	−50.2	4.9	57.5	10.2
	Sandstone	YAN07	42.3921	69.5396	3/4	359.6	−53.6	2.9	24.2	25.6	81.8	108.0	192/17	23.1	−53.8	2.9	24.1	25.7
	Mudstone	YAN09	42.3974	69.5429	6/6	322.8	−53.1	5.9	44.8	10.1	59.7	24.8	192/17	344.9	−63.8	5.9	44.7	10.1
				Mean values	7/7	347.5	−53.2	6.9	77.6	6.9				338.6	−60.6	6.9	40.0	9.7
B	Tuff	CCG01	43.1561	69.2517	5/5	0.2	−44.2	4.9	50.3	10.9	72.8	111.2	205/11	11.5	−47.0	4.9	41.0	12.1
	Tuff	CCG02	43.1566	69.2518	6/6	346.5	8.8	5.9	66.2	8.3	−40.9	92.9	280/16	346.7	−5.9	5.9	66.0	8.3
	Mudstone	CCG03	43.1859	69.2279	7/7	1.5	−48.2	6.8	24.9	12.3	76.0	116.2	312/16	345.1	−58.9	6.8	24.9	12.3
				Mean values	2/3	0.8	−46.2	2.0						359.8	−54.1	2.0		
F	Sandstone	PEQ01	43.2923	68.9929	7/7	2.5	−50.3	6.6	16.6	15.2	77.6	121.2	245/30	45.2	−71.7	6.6	16.7	15.2
		PEQ02	43.2907	68.9934	5/5	15.7	−55.5	4.8	23.1	16.3	75.9	175.1	245/30	71.2	−68.2	4.8	23.2	16.2
		PEQ03	43.2905	68.9962	3/3	298.3	−64.9	2.9	24.6	25.4	47.4	353.8	245/30	213.0	−72.6	2.9	24.6	25.4
		PEQ05	43.2910	68.9952	3/4	318.3	−31.6	3.0	41.9	19.3	46.2	44.4	245/30	306.2	−59.6	3.0	42.1	19.2
				Mean values	2/4	8.7	−53.1	2.0	146.0	20.8				59.3	−70.4	2.0	146.1	20.8
	Sedimentary units			Mean values	16/16	355.7	−54.4	15.8	71.4	4.4				4.2	−56.7	15.1	16.1	9.5

south from khaki-coloured mudstones. In total, 19 samples were collected from these sites (see Fig. 2b and Table 2).

(c) The last sampling area is located to the west of the El Quemado Post, specifically at its type locality, the Calcáreo Canyon (F area, PEQ sites; Figs 1b and 2f). Here, coarse-grained sandstones with pale yellow colour and reddish patches were sampled (Fig. 3h). These units were challenging to sample because they easily break apart. A total of 33 samples were obtained from five sites (Table 2). It should be noted that sites PEQ03 and PEQ04 likely correspond to the overlying Chubut Group, as indicated by Volkheimer *et al.* (2009).

2.2 Palaeomagnetic and rock magnetic methods

Rock magnetic studies were conducted using representative samples of the studied lithologies to investigate the origin of the natural remanence (NRM) and identify the ultimate carriers of remanent magnetism (Fig. 4). Raw data from these experiments can be found in Appendices A (sedimentary units) and B (volcanic units).

Isothermal remanent magnetization (IRM) acquisition curves, backfield demagnetization of saturation IRM (SIRM) curves, and hysteresis loops were performed with a Kazan University (Russian Federation) J-Meter coercivity spectrometer (Jasonov *et al.* 1998) at the Complutense University of Madrid and a Molspin Ltd vibrating sample magnetometer at the University of Buenos Aires (only the L3-5 sample). The thermomagnetic susceptibility versus temperature curves were conducted using a CS-3 attachment for the *AGICO* MFK1-FA Kappabridge in Buenos Aires laboratory and a KLY-4S Kappabridge in Madrid.

Most samples were demagnetized thermally (TH), applying progressively higher temperatures until the samples were completely demagnetized (Butler 1992). Additionally, demagnetization by alternating fields (AF) were performed as pilot tests at every site. However, in CCG samples, only AF demagnetization was employed. This approach was chosen as the demagnetization results were equivalent to those obtained with the thermal method and applying AF alone guaranteed complete demagnetization of these samples (see Fig. 5e). Thermal demagnetization was performed using ASC Scientific TD-48 SC and Magnetic Measurements MMTD thermal demagnetizers in the Buenos Aires and Madrid laboratories, respectively. In Buenos Aires, an *AGICO* LDA-3A rotating demagnetizer for alternating magnetic fields was used, while an *AGICO* JR6 rotating magnetometer was employed for the remanence measurements. In Madrid, a 2 G superconducting magnetometer equipped with SQUID-DC SSR sensors, and an in-line AF demagnetizer was used. Bulk susceptibility measurements during heat treatment were conducted to monitor any mineral transformation. These measurements were performed using a *Bartington* susceptibilimeter in Buenos Aires. (see Appendix C). To ensure accuracy, all directions were corrected for the current declination of the Earth's magnetic field (EMF). Characteristic remanent magnetizations (ChRM) were determined averaging at least four demagnetization steps, with a mean number of steps per ChRM of seven. This ensured a maximum angular deviation of less than 10°, averaging 6° (Kirschvink 1980). The complete ChRM data can be found in Appendix D.

2.3 Palaeomagnetic and rock magnetic results

The results of the demagnetization of the samples reveal that the magnetic remanence is hosted by minerals with high coercivity and high unblocking temperatures. As can be observed in the Zijderveld diagrams (Zijderveld 1967; Fig. 4a), the directions of the remanence components are easily identifiable, pointing towards the origin and showing low dispersion. Furthermore, in the demagnetization diagrams (Fig. 4b), it can be noted that the magnetic remanence persists even under high AF (100 mT) and high temperatures (above 580 °C).

Therefore, observing all the experiments, it can be asserted that the studied rocks, both volcanic and sedimentary, contain low-Ti titanomagnetite and pure magnetite as the main carrier of magnetic remanence and, to a lesser extent, haematite (Fig. 4c). In addition to these minerals, the results indicate the presence of paramagnetic and superparamagnetic (SP) minerals, (titano)maghemite and sulfides. The slope of the magnetic hysteresis loop after saturation indicates the presence of paramagnetic minerals (Fig. 4d), while SP minerals can be recognized in the Day-plot (Day *et al.* 1977; Dunlop 2002; Fig. 4e). The presence of (titano)maghemite and sulfides is discernible during the heating curve in the thermomagnetic curves, showing a peak between 200 and 400 °C and an increase in susceptibility between 400 and 500 °C, respectively (Jagadeesh & Seehra 1981; Moskowitz 1981; Martín-Hernández *et al.* 2008; Fig. 4f).

2.3.1 Lonco Trapial Group

In the samples collected from the A area (LTE, eight sites, see Figs 1b and 2a), two distinct remanence components were identified after removing a viscous remanent magnetization (VRM; Fig. 5). The details are as follows:

(i) In most of the samples, a low-temperature component (L) was isolated between 200 and 450 °C, or 5 and 30 mT (Fig. 5a). However, in LTE02, 04, 06, 07 and 08 sites, the dispersion ($k < 10$; Van der Voo 1990) or the lack of a minimum of directions did not allow the calculation of mean values per site.

(ii) A high-temperature component (M) was isolated between 450 and 680 °C, except for LTE08 samples, in which the M component was determined between 450 and 580 °C.

(iii) In the LTE08 site samples, a very high-temperature component (H) was identified, ranging between 580 and 680 °C. However, due to a lack of a sufficient number of demagnetization steps, it could not be precisely determined.

The remanence directions of the M component exhibit both positive (reverse inclination in the Southern hemisphere) and negative (normal inclination in the Southern hemisphere) inclinations. In contrast, the L component directions exclusively have negative inclinations (see Fig. 5a). Using the M components, a total of six mean directions were calculated. However, the mean directions from the LTE04 and LTE07 sites were discarded due to an unacceptable kappa value ($k < 5$; Van der Voo 1990). Three mean directions were calculated with the L components (see Table 3). Finally, virtual palaeomagnetic poles were calculated for each mean direction (Table 1).

In the B area (LTG, five sites, see Figs 1b and 2b), two ChRM components were identified in the samples after removing a VRM. The details are as follows:

(i) An L component was also identified within the temperature range of 200–400 °C, or an AF field range of 2–60 mT (Fig. 5b).

(ii) Between 400–580 °C, or 2–60 mT, to 550–680 °C, an M component was determined (Fig. 5b). These differences between the unblocking temperatures of the M component can be attributed to the lithological differences within the LTG sites (see section 2.1).

The directions of the M component exhibit both positive and negative inclinations, whereas the directions of the L component

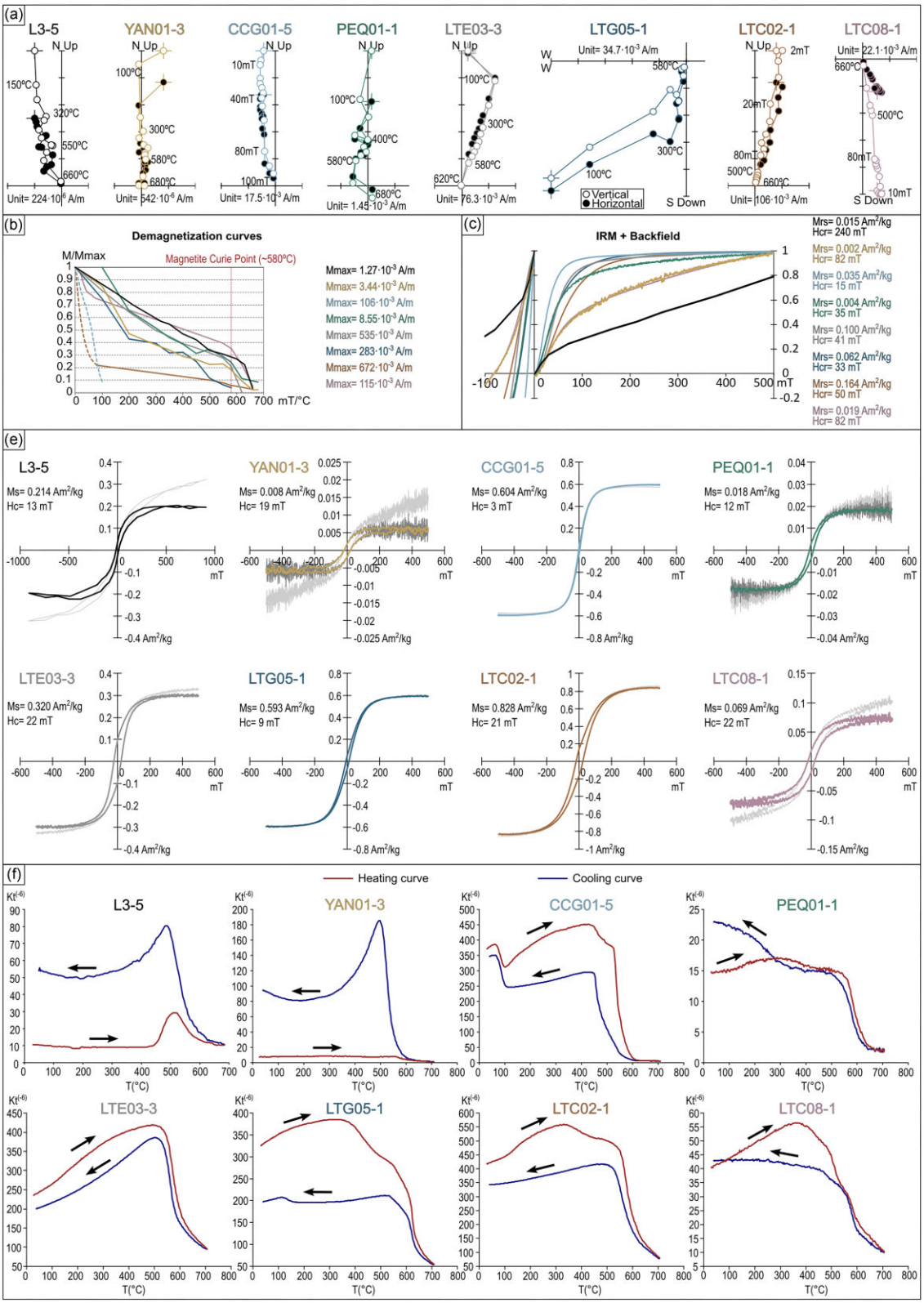

Figure 4. Palaeomagnetic and rock magnetic studies. The L3-5 sample corresponds to a fine-grained sandstone of the Las Leoneras Formation (see Fig. 2d). The CCG01-5 and YAN01-3 samples are tuffaceous sandstones, and the PEQ01-1 sample corresponds to coarse-grained sandstone, of the Cañadón Calcáreo Formation (see Figs 2b, e and f). The LTE03-3, LTG05-1, LTC02-1 and LTC08-1 samples are an andesitic dyke, an ignimbrite, a lava and an autobrecciated lava, respectively, of the LTG (see Figs 2a–c). (a) Orthogonal diagrams of the selected representative samples. (b) Thermal demagnetization curves of the NRM from (a) samples. (c) IRM and backfield with the saturation remanence (Mrs) and remanent coercive force (Hcr). L3-5 sample is out of the graphic because the IRM was done to a peak field of 1T. (d) Hysteresis loops with saturation magnetization (Ms) and coercive force (Hc). The grey line corresponds to the raw loop, and the dashed line to the uncorrected loop. (e) Thermomagnetic curves (susceptibility versus temperature).

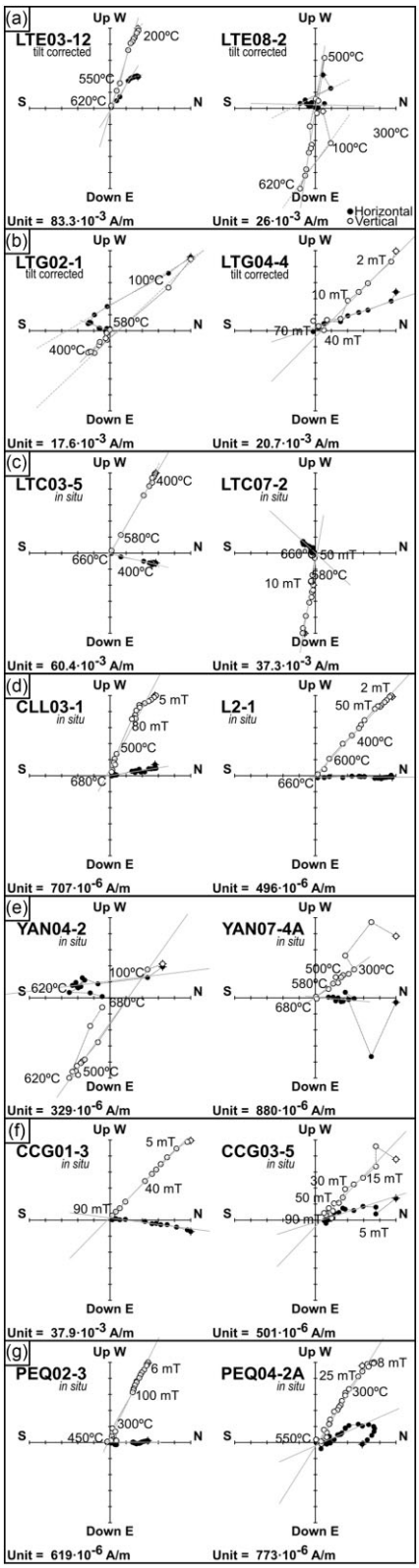

Figure 5. Orthogonal demagnetization diagrams (Zijderveld 1967) of some samples. The LTG (a) in the A area; (b) in the B and (c) in the C area. The Las Leoneras Formation (d) in the D area. The Cañadón Calcáreo Formation (e) in the E area; (f) in the B area and (g) in the F area. The ChRM directions of the M component are marked with a solid line and the L component with dashed line.

exclusively have negative inclinations (Fig. 5b). Furthermore, the virtual palaeomagnetic poles for each site in the B area were calculated (Table 1).

In the C area (LTC, 13 sites, see Figs 1b and 2c), the following remanence components were isolated from the samples:

(i) The M component was determined between 200 °C, or 5 mT, and 580–680 °C (Fig. 5c).

The directions of the M component in the LTC area have both positive and negative inclinations. However, in this case, the inclination of the layers was not assumed to be the result of a tilted bedding plane because tilt ranges from 25° to 30° are typical for a cinder cone (e.g. Wood 1980; Rodríguez-González & Fernández-Turiel 2015). Moreover, after applying the tilt corrections, the mean directions of positive polarities disperse instead of grouping ($k = 112$ before correction and $k = 88$ after correction). Therefore, M component mean directions and a reversal test were calculated in geographical coordinates. Both the McFadden & Lowes (1981) and McFadden & McElhinny (1990) reversal tests indicate that the positive and negative mean directions do not share a common mean at 95 per cent confidence ($\gamma_c = 25.76°$ and $\gamma_o = 7.29°$). Therefore, these results may imply that palaeosecular variation may not be averaged in the LTC units (Fig. 6b). Likewise, a VGP was calculated for each site (Table 1).

Assuming that the site LTC had experienced a different tectonic setting than LTG and LTE, a reversal test (McFadden & McElhinny 1990) was conducted using the mean directions of the M components from LTE and LTG sites. The test resulted in a positive class C ($\gamma_c = 18.1°$ and $\gamma_o = 14.9°$), with a common mean at 95 per cent confidence (McFadden & Lowes 1981). A new reversal test by Heslop *et al.* (2023) was also conducted, and it indicates that the *Y* component of the mean of positive and negative directions of LTG–LTE sites does not match, but the angle between means is smaller than 14.5° (Fig. 7a). Similarly, the test points out that the *Z* component of the mean directions of LTG and LTE does not match, but the angle between means is smaller than 14.5° (Fig. 7b). Despite the lack of a perfect match, we assume that the angular deviation between means is acceptable. Each site of the LTG units corresponds to a single lava flow or ignimbrite, which may represent spot readings of the EMF, but their dispersion and the positive reversal tests in the LTE–LTG units indicate that the palaeosecular variation was averaged out, representing enough time span to give a representative palaeopole. (Fig. 6a).

2.3.2 *Las Leoneras Formation*

Two ChRM components were determined after removing a VRM in the samples from the D area (CLL and L, eight sites, see Figs 1b and 5d). The details are as follows:

(i) In most of the samples the M component was completely demagnetized at a temperature of 680 °C.

(ii) Only in three samples an H component could be isolated within the temperature range of 400–500 and 630–680 °C.

All the directions of the M component of the Las Leoneras Formation samples present negative inclinations. In contrast, the directions of the M component of the LTG site (CLL01) samples and the H component of both the Las Leoneras Formation's samples and CLL01 samples present positive inclinations.

Therefore, it is assumed that the sill of the LTG did not remagnetize the units of the Las Leoneras Formation. The mean directions

Table 3. Statistical parameters (Fisher 1953) of the L component remanence directions from the units of the LTG. n/N = used samples/total samples.

Site	n/N	Site coordinates		Geographic coordinates					VGPs	
		Lat. (°S)	Long (°E)	Dec.	Inc.	R	k	$\alpha 95$ (°)	Lat. (°S)	Long. (°E)
LTE01	3/4	42.9067	69.2990	1.2	−45.0	3.0	114.9	11.6	73.7	114.4
LTE03	3/3	42.9068	69.2992	354.5	−70.4	3.0	86.0	13.4	77.8	305.8
LTE05	3/3	42.9103	69.3009	357.7	−59.7	2.9	28.3	23.6	87.1	73.5
LTG02	4/4	43.1905	69.2428	347.3	−54.6	4.0	74.0	10.8	77.4	55.9
LTG03	4/4	43.1859	69.2309	354.5	−60.5	4.0	113.3	8.7	85.6	42.1

of the H component were discarded because $k < 10$ (Van der Voo 1990). Mean directions were calculated using the M component for each site within the Las Leoneras Formation (Fig. 6c), while the mean direction of the M component of the CLL01 site has an unacceptable ($k < 10$; Van der Voo 1990). These mean directions are summarized in Table 2.

2.3.3 *Cañadón Calcáreo Formation*

In the E area (YAN, nine sites, Figs 1b and 2e), all the samples present a VRM, which was obliterated above 150 °C. After removing the VRM samples revealed the following:

(i) Between the first or second step of demagnetization and 680 °C, an M component was determined in the samples without the H component (Fig. 5e).

(ii) An H component was present in half of the samples after removing the M component at 450°. The H component was isolated between 450 and 680 °C (Fig. 5e). However, the MAD of most of those directions exceeded the acceptable threshold (MAD > 10°; Kirschvink 1980).

The inclinations of the M component are all negative. In contrast, the inclinations of the H component are all positive, but the demagnetization steps were not sufficient (< 4) to determine those components (Fig. 5e). A mean direction of the M component was calculated for each site (Table 2), excluding the YAN03 and YAN08 sites ($k < 10$; Van der Voo 1990). After applying the tilt correction, the clustering of remanence directions diminishes (geographic coordinates $k = 78$ and stratigraphic coordinates $k = 40$; Fig. 6d). To assess this further, a fold test was conducted (McFadden 1990) yielding a non-significant result ($p = 0.05$ and CR = 2.69). Thus, it is presumed that the remagnetization occurred after the folding process.

The samples from the B area (CCG, three sites, see Figs 1b and 2b), located to the south of the Gorro Frigio Peak (Figs 1 and 2c), were primarily demagnetized by AF on the basis that the thermal method showed consistent results (one specimen per site was demagnetized by thermal method). The details are as follows:

(i) After removing a VRM, the M component was determined between 5 and 100 mT (Fig. 5f).

The M component consistently displays negative inclinations in all the samples. Mean directions for each site were calculated, with six to seven directions per site (Table 2). The CCG02 site was discarded due to its anomalous direction (Fig. 6e). Furthermore, when tilt corrections are applied to the remanence directions the angular distance between them increases (4.1° before correction and 18.8° after correction). Consequently, a tilt test (McFadden 1990) was performed using CCG01 and CCG03 sites, resulting in a statistically significant and negative outcome ($p = 0.05$ and CR = 19). Hence, it is postulated that the magnetization was acquired after the tilting.

The last sites of the Cañadón Calcáreo Formation in the F area (PEQ, five sites, Figs 1 and 2g) presented:

(i) After removing a VRM, an M component was determined from the first demagnetization step to the complete demagnetization of the sample (Fig. 5g).

(ii) In just two samples, after the M component (isolated up to 580 °C), an H component was characterized from 580 °C to the complete demagnetization (Fig. 5g).

Mean directions of H components were discarded for being insufficient ($n < 3$; Fisher 1953). Like the previous cases, the M remanence directions consistently displayed negative inclinations (see Fig. 5g). Mean directions were calculated for the M components (Table 2), but site PEQ04 was disregarded ($k < 10$; Van der Voo 1990; Table 2). Additionally, sites PEQ03 and PEQ05 were also excluded because of their anomalous direction, with an angular deviation of more than 35° from the other two mean directions (Fig. 6f). As all the units have the same bedding plane, it was not possible to calculate a tilt or fold test.

3 DISCUSSION

3.1 Remagnetization of the sedimentary units of the CAB

The Jurassic period is well known for experiencing a high rate of geomagnetic field reversals (e.g. Biggin *et al.* 2012; Kulakov *et al.* 2019). However, these are not well preserved in the magnetic remanence of the studied sedimentary units (see Figs 5 and 6). The remanence directions of the Las Leoneras and Cañadón Calcáreo formations only show normal (negative) inclinations of the M component, which is unexpected because of the extent of the sampling area (see Fig. 1), the age range (ca. 189 to 157 Ma, Cúneo *et al.* 2013) and the number of sites (26 sites; see Fig. 2). Additionally, the sampled sites of the sedimentary units in the CAB correspond to different beds rather than different strata. Therefore, it is highly unlikely that the high value of the kappa parameter is attributable to spot readings of the field during the formation of the rocks but is instead related to a remagnetization of these units during a hydrothermal stage (see Fig. 1c). Moreover, when the tilt corrections of each site are applied, the mean directions disperse instead of grouping (Fig. 7a). Also, the L component of the LTG units presents similar directions in comparison with the ones obtained in the sedimentary units of the CAB in *in situ* coordinates (without applying any tilt correction; see Table 3 and Fig. 8a).

Hence, a tilt test was performed with the mean directions (McFadden 1990), giving a negative result: $p = 0.05$; CR = 1.69; $k = 72.6$ *in situ* and $k = 16.7$ tilt corrected (Fig. 9). In this regard, the L component is carried by a different grain size fraction or compositional type (see Fig. 4f; Huang *et al.* 2023) with the unblocking temperature at 450 °C (see Section 2.3.1). Therefore, these remanence directions are post-tectonic, and an overall remagnetization

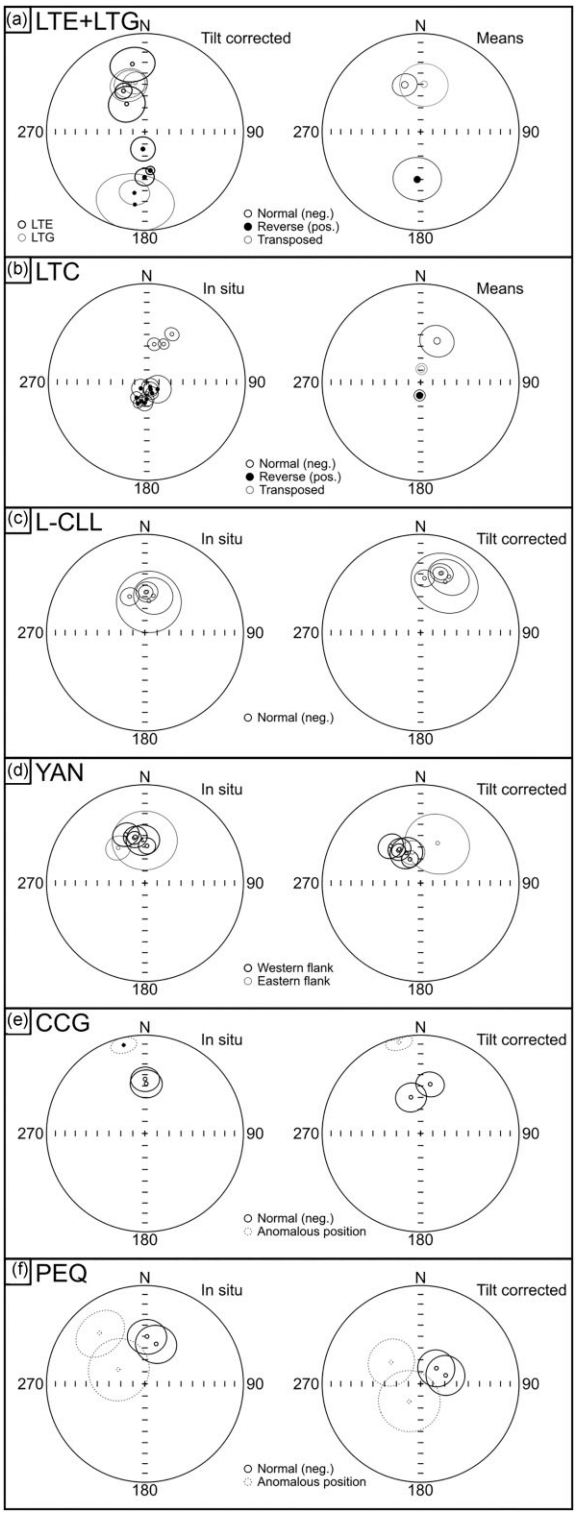

Figure 6. Stereographic projection of the mean directions per site. LTG means (a) from the A and B area, and (b) from the C area. The reverse mean direction (black circle) is transposed to the normal position (grey circle) for comparison with the normal mean (empty black circle). (c) Cañadón Las Leoneras Formation means per site from the D area. Cañadón Calcáreo Formation means (d) from the E area, the synclinal fold near Yanquetruz Post, with the means of the western flank marked with a bold line and those of the flank marked with a thin line; (e) from the B area and (f) from the F area. Discarded means for being in an anomalous position are marked with a dotted line.

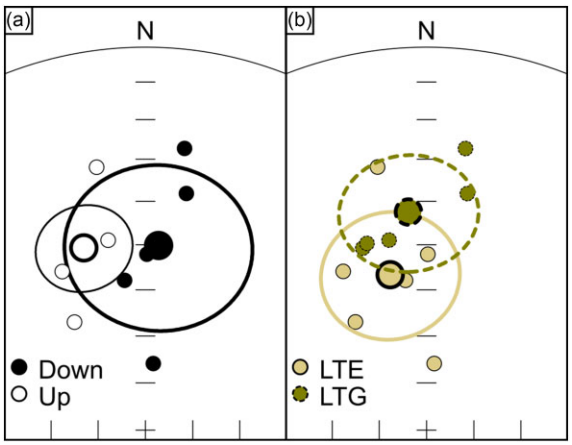

Figure 7. Stereographic projection of the mean directions of the LTG and LTE sites: (a) positive (down) and negative (up) mean directions of both sites plotted in the same polarity; and (b) mean directions of LTG (dashed line) and LTE (solid line) sites.

is inferred, as proposed by Geuna *et al.* (2000) for some localities of the CAB. A palaeomagnetic pole was calculated with the VGPs of each site, which statistical parameters are (Fisher 1953): $N = 21$, Lat. = 82.7°S, Long. = 82.5°E, $K = 44.8$ and $A95 = 4.8°$ (Fig. 8b).

Several mineral and hydrothermal deposits are described along the CAB (e.g. Fernández Lima & Latorre 1978), primarily associated with the genesis of the LTG and the volcanic units of the Cañadón Asfalto Formation (Márquez *et al.* 2016; Bouhier *et al.* 2017). Additionally, some mineralized veins are reported within the units of the Cañadón Calcáreo Formation (Fernández Lima & Latorre 1978; Sangster 2001; Fig. 8c). In this work, we identified that some of the units were recrystallized in the Las Leoneras Canyon (D area), a patina of malachite was appreciable in the walls of some veins in outcrops of the cinder cone (C area), and some mineralized veins were abundant within the units of the Cañadón Calcáreo Formation near the Yanquetruz Post (E area; see Fig. 8c). These recrystallized areas were avoided during the sampling, but the evidence presented here suggest that hydrothermal fluids may have affected the units beyond those areas.

To determine the potential age of the remagnetization within the studied area of the CAB, the palaeomagnetic pole was compared to the Jurassic South American Apparent Polar Wander Path (APWP) of Ruiz González *et al.* (2022) and the global Jurassic APWP means of Vaes *et al.* (2023; Table 4 and Fig. 10). Based on this, the polar direction of the mean pole in relation to these APWPs suggests that the hydrothermal stage which triggered the remagnetization of the studied units could have occurred around 145 Ma (see Fig. 10). This is consistent with the fact that mineralized veins must be younger than ca. 157 Ma (Cúneo *et al.* 2013) since they cut through the units of the Cañadón Calcáreo Formation (see Fig. 8c).

In the same way, the dating of zircons in units of the Cañadón Calcáreo Formation near to the El Torito Ranch (see Fig. 1b) yielded a U-Pb age of 157.387 Ma (Cúneo *et al.* 2013) whereas a K-Ar age in biotite of 147.1 Ma from the same formation (Cabaleri *et al.* 2010) suggests the resetting of ages due to the hydrothermal activity or a mixture of signs due to a K problem. Also, in units from the LTG, whole rock K-Ar dates of 147 and 136 Ma also have been reported (Nullo 1978, 1983). This age range is confirmed by the absence of this type of mineralization in the Cretaceous formations (Sangster 2001; Márquez *et al.* 2016).

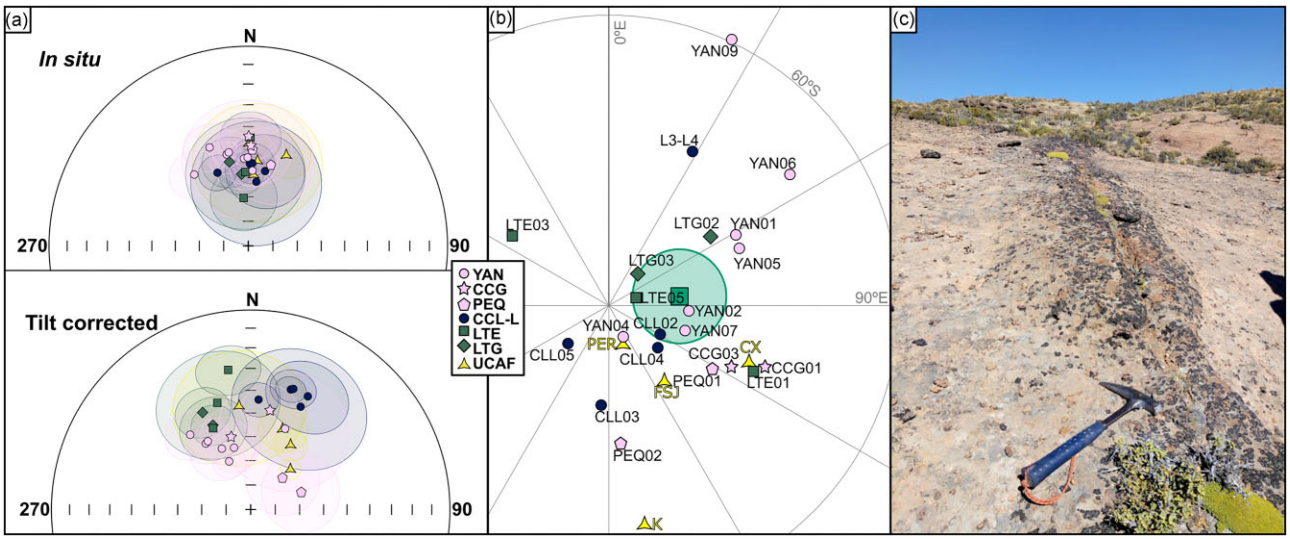

Figure 8. Projection of the M component from the sedimentary units (Las Leoneras and Cañadón Calcáreo formations) and the L component from the LTG units: (a) stereographic projection of the mean directions, with the means of the Cañadón Calcáreo Formation (YAN, CCG and PEQ), Las Leoneras Formation (CLL-L) and Lonco Trapial Group (LTE and LTG). In addition, the mean directions of Geuna *et al.* (2000), Upper Cañadón Asfalto Formation in their text (UCAF) are plotted in triangles. (b) Geographic projection of the VGPs calculated with the *in situ* means (same shapes as in a), the mean palaeomagnetic pole is marked with a square and (c) mineralization veins cutting the Cañadón Calcáreo Formation in the E area, near the Yanquetruz Post, between sites YAN07 and YAN09 (see Figs 1b and 2e).

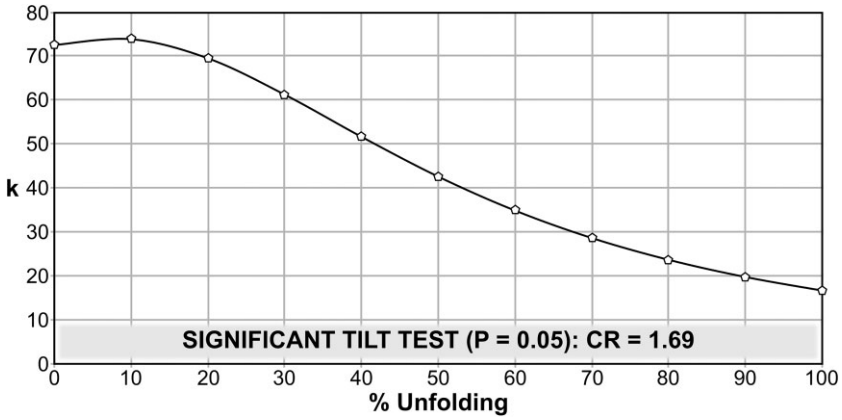

Figure 9. Fold (tilt) test by McFadden (1990). It can be observed that at 10 per cent tilting, the parameter *k* slightly increases, but it decreases as the tilting is progressively applied.

Table 4. Geographic coordinates and statistical parameters (Fisher 1953) of the Jurassic mean directions of the South American APWP of Ruiz González *et al.* (2022) and the global APWP of Vaes *et al.* (2023), both in South American coordinates (see Fig 10b).

Age (Ma)	Ruiz González *et al.* (2022)					Vaes *et al.* (2023)				
	N	Lat. (°S)	Long. (°E)	*K*	*A*95 (°)	*N*	Lat. (°S)	Long. (°E)	*K*	*A*95 (°)
200	4	80.4	243.1	178.3	6.9	705.9	78.9	245.0	9.6	1.8
190	4	80.1	217.7	879.4	3.1	117.8	77.4	217.1	28.1	2.5
180	3	82.1	198.1	138.9	10.5	243.7	81.4	214.8	23.5	1.9
170	2	83.0	176.3	156.5	20.1	44.8	88.4	228.8	13.2	6.1
160	4	84.0	179.3	1159	2.7	68.5	87.5	160.1	17.6	4.2
150	5	85.3	154.0	163.6	6	76.3	85.3	85.0	16.6	4.1
140	11	86.1	73.8	578.5	1.9	125.3	83.7	64.1	33.8	2.2

Taken into account the previous ages, it is interpreted that the origin of the mineralizations were triggered by an extensional stage of the CAB, which facilitated the hydrothermal activity through an extended and thinned crust (e.g. Foley *et al.* 2023). This extensional stage correlates with the change in the direction of the continental drift of South America, from a clockwise rotation of the whole continent to a westward drift (Somoza & Zaffarana 2008; Ruiz González *et al.* 2022). In the CAB, this also coincides with the deposition of the K megasequence (Figari *et al.* 2015), due to the generation of accommodation space during the thermal subsidence

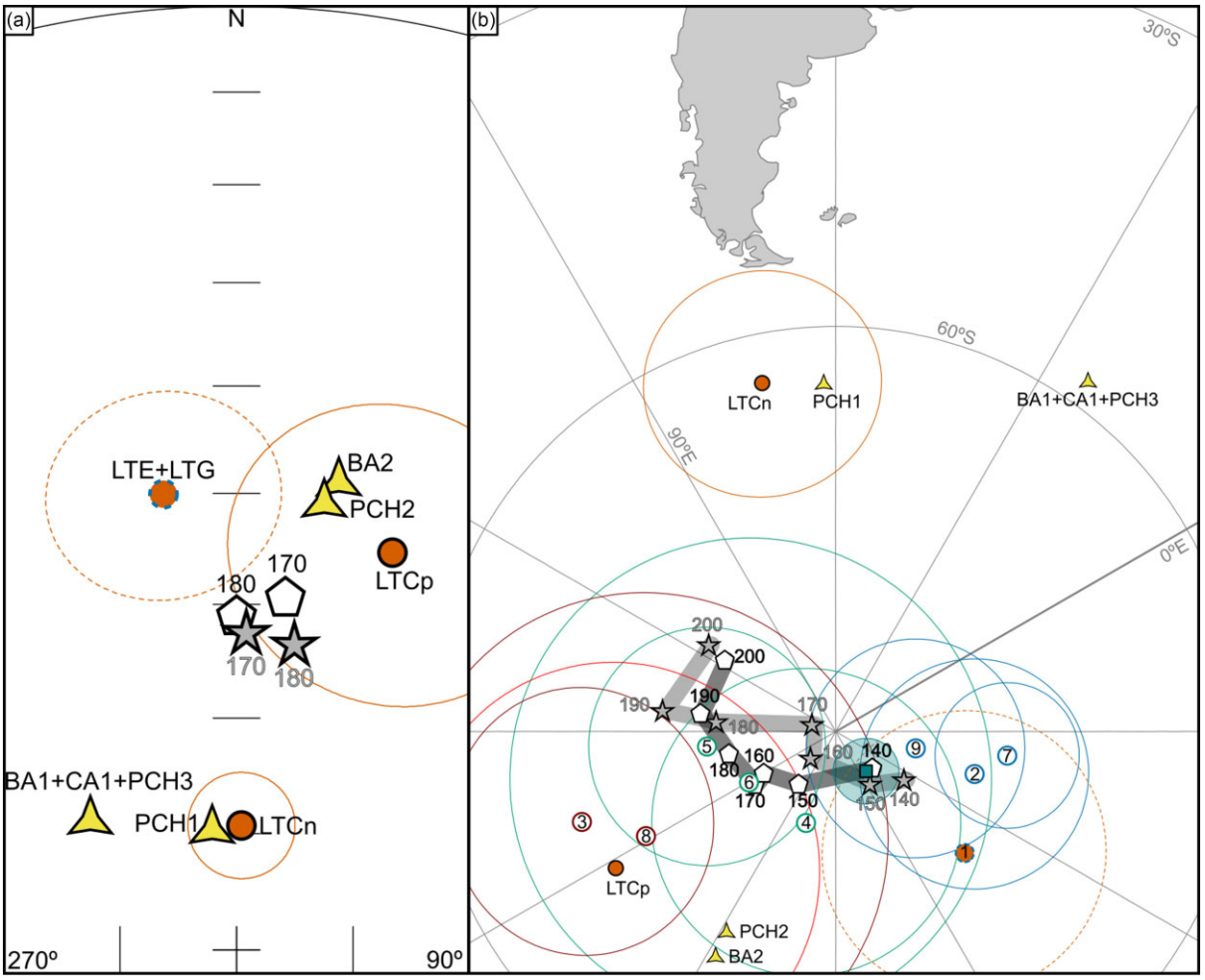

Figure 10. (a) Stereographic projection of the LTG mean directions calculated in this work correspond to the circles, the LTC means also are presented with solid lines (LTCn) and dashed lines (LTCp, see Table 5). The mean directions obtained by Geuna *et al.* (2000) from the volcanic units of the (Lower) Cañadón Asfalto Formation correspond to the triangles. Also, the Jurassic mean directions of 180 and 170 Ma from the South American APWP of Ruiz González *et al.* (2022) and global APWP of Vaes *et al.* (2023) correspond to the pentagons and stars, respectively. (b) Poles calculated from the mean directions from a) have the same shape scheme. Also, the Jurassic (190–140 Ma) mean poles of the APWP of Ruiz González *et al.* (2022) and GAPWP of Vaes *et al.* (2023) are included. The palaeopole of the remagnetized units corresponds to the square. In addition, other Early Jurassic poles from Patagonia are included to compare with those obtained in this work. From the North Patagonian Massif: (1) Lonco Trapial Group (this work), (2) Lonco Trapial Group (Zaffarana & Somoza 2012), (3) Mamil Choique dykes (Rapalini & Lopez de Luchi 2000), (4) Marifil Formation (Iglesia Llanos *et al.* 2003), (5) Marifil Complex (Vizán 1998) and (6) Marifil dykes (Rapalini & Vilas 1991). From the Deseado Massif (southern Patagonia): (7) Chon Aike Formation, (8) Bajo Pobre Formation (Ruiz González *et al.* 2022), and (9) Chon Aike Formation (Vilas 1974). The poles 2, 7 and 9 indicate anticlockwise rotations about vertical axis, tand 3 and 8 indicate clockwise rotations, and 4, 5 and 6 indicate no rotations.

stage of the basin. Furthermore, this mean pole does not indicate any rotation about vertical axis because, as presented earlier, the directions of the remanence are better grouped *in situ* and scatter when tilt corrections are applied (see Fig. 8a). It lies within the *A*95 confidence ellipse of the 150 and 140 Ma mean poles (Fig. 10). This suggests that, at least since approximately 145 Ma, the strain within the area did not contain a shear component.

On the other hand, the age of the obtained pole is constrained between the Oxfordian and Aptian (Geuna *et al.* 2000; Cúneo *et al.* 2013), so it would have been recorded by remagnetization if there had been a significantively large True Polar Wander event such as the 'Monster shift' in that timeframe (e.g. Kent & Irving 2010). Therefore, there are no indications of such an event in the studied units, and its existence is disputed.

Although the sedimentary units analysed in this study show an intense remagnetzsation, Geuna *et al.* (2000) documented a clockwise rotation of the Gorro Frigio. Interestingly, this rotation was observed in units equivalent to those from the C and F areas in this study (see Fig. 11a). In the CX and K sites in Geuna *et al.* (2000), the Cañadón Calcáreo Formation (Upper Cañadón Asfalto Formation *sensu* Geuna *et al.* 2000) was sampled revealing positive and negative directions, which could imply that the sampled units in that study did not suffer a single remagnetization event. However, the mudstones and fine-grained sandstones from CX and K sites showed a soft magnetization which was eliminated at 30 mT or 400 °C and in some samples was the only component (see Geuna *et al.* 2000).

Additionally, as can be seen in Fig. 10, the mean directions obtained by Geuna *et al.* (2000) exhibit a significant clustering when projected onto *in situ* coordinates. This could be attributed to the possibility that, similar to the sedimentary units studied in this work, they might have undergone remagnetization through an event that

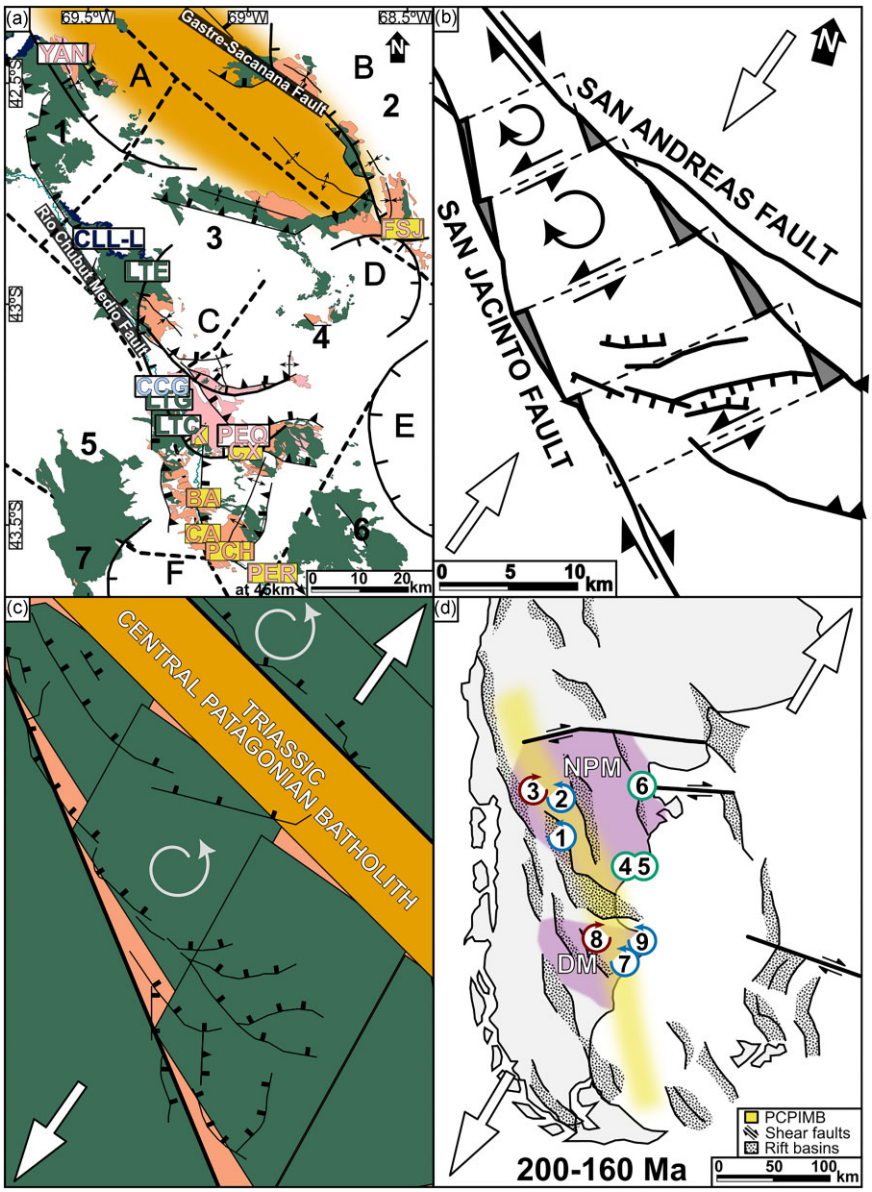

Figure 11. (a) Geological map of the study area featuring the sampled sites of this study (black squares) and those by Geuna *et al.* (2000; yellow filled squares). The region of the Central Patagonian Batholith and the Gastre Basin Block is highlighted in mustard colour (Ruiz González *et al.* 2020). The depocentres identified by Figari *et al.* (2015) are labelled with capital letters: (A) Gastre, (B) Gan-Gan, (C) Gorro Frigio, (D) Fossatti, (E) General Racedo and (F) Paso de Indios. The crustal domains proposed by Renda *et al.* (2019) are marked with numbers: (1) Gastre, (2) Lonco Trapial, (3) Taquetrén, (4) Pichiñanes, (5) Piedra Parada, (6) Los Altares and (7) San Bernardo. Adapted from Bilmes *et al.* (2013), Cúneo *et al.* (2013), Figari *et al.* (2015), Allard *et al.* (2021b) and Ardolino *et al.* (2022). (b) Model depicting shear-driven rotation of blocks near the convergence of the San Andreas and San Jacinto Faults (southern California) within the broader San Andreas Fault System (modified from Nicholson *et al.* 1986). White arrows represent the extensional stress direction. (c) Schematic model illustrating the block dynamics during the Jurassic extension of the CAB. Grey arrows indicate the block rotations reported by Zaffarana & Somoza (2012; upward) and this study (centre), while (d) Early to Middle Jurassic extensional model (modified from Uliana *et al.* 1989), encompassing the Palaeozoic Central Patagonian Igneous–Metamorphic Belt (Renda *et al.* 2019, 2021), and the locations of palaeomagnetic studies on Lower to Middle Jurassic units: (1) Lonco Trapial Group (this study), (2) Lonco Trapial Group (Zaffarana & Somoza 2012), (3) Mamil Choique dykes (Rapalini & Lopez de Luchi 2000), (4) Marifil Formation (Iglesia Llanos *et al.* 2003), (5) Marifil Complex (Vizán 1998), (6) Marifil dykes (Rapalini & Vilas 1991), (7) Chon Aike Formation, (8) Bajo Pobre Formation (Ruiz González *et al.* 2022) and (9) Chon Aike Formation (Vilas 1974). Poles with a blue line indicate anticlockwise rotations about the vertical axis, those with a maroon line indicate clockwise rotations, and those with a green line indicate no rotations. North Patagonian Massif (NPM) and Deseado Massif (DM) are highlighted in purple.

lasted long enough to record directions of both polarities or, alternatively, through multiple events over time, given the still high frequency of reversals during that period (e.g. Doubrovine *et al.* 2019).

3.2 Palaeomagnetic record of the Jurassic deformation of the CAB

One of the main discussions about the CAB is the nature and tectonic setting of the basin (Silva Nieto *et al.* 2005; Figari *et al.* 2015; Allard

Table 5. Geographic coordinates and statistical parameters (Fisher 1953) of the poles obtained from the units of the Lonco Trapial Group (upper part). Also, the magnetic directions and the tectonic motions calculated with the obtained poles and the mean poles of Ruiz González *et al*. (2022) and Vaes *et al*. (2023) with the method developed by Beck (1976; 1980), Demarest (1983) and Beck *et al*. (1986). Possible motions, those with a degree bigger than the uncertainty, are highlighted in grey.

Pole	Area	Age (Ma)	Correction	N	Lat. (°S)	Long. (°E)	K	A95 (°)
LTE+LTG	A+B	185 - 172	Tilt corrected	11	77	73.3	20.2	10.4
LTCn	C	185 - 172	*In situ*	3	71.0	178.2	69.5	14.9
LTCp	C	185 - 172	*In situ*	10	63.7	288.1	33.3	8.5
Calculated tectonic motions relative to the poles of the South American APWP by Ruiz González et al. (2022)								
Lonco Trapial Group		**180 Ma**				**170 Ma**		
		Expected direction	**Obtained direction**	**Apparent Rotation**	**Expected direction**	**Obtained direction**	**Apparent Rotation**	
LTE+LTG	A+B	D = 10.7; I = −61.1	D = 351.3; I = −49.7	20.0° ± 13.8°	D = 8.3; I = −59.0	D = 351.3; I = −49.7	17.6° ± 21.2°	
LTCn	C	D = 10.7; I = −61.3	D = 21.7; I = −52.8	10.5° ± 16.8°	D = 8.3; I = −59.3	D = 21.7; I = −52.8	12.9° ± 23.4°	
LTCp	C		D = 4.1; I = −79.2	7.3° ± 20.7°		D = 4.1; I = −79.2	4.9° ± 26.3°	
Calculated tectonic motions relative to the poles of the Global APWP byVaeset al. (2023)								
Lonco Trapial Group		**180 Ma**				**170 Ma**		
		Expected direction	**Obtained direction**	**Apparent Rotation**	**Expected direction**	**Obtained direction**	**Apparent Rotation**	
LTE+LTG	A+B	D = 11.7; I = −63.0	D = 351.3; I = −49.7	21.0° ± 9.2°	D = 2.0; I = −62.4	D = 351.3; I = −49.7	11.3° ± 10.9°	
LTCn	C	D = 11.8; I = −63.3	D = 21.7; I = −52.8	9.4° ± 13.3°	D = 2.0; I = −62.7	D = 21.7; I = −52.8	19.3° ± 14.6°	
LTCp	C		D = 4.1; I = −79.2	8.4° ± 18.0°		D = 4.1; I = −79.2	1.5° ± 18.9°	

et al. 2021a). In this context, it has been proposed to be a pull-apart basin (Silva Nieto *et al.* 2005) or an extensional basin with depocentres as half-grabens that were generated by tectonic block rotations (Geuna *et al.* 2000; Figari *et al.* 2015). For this purpose, the palaeomagnetic method is a unique tool for unravelling the deformation recorded by the tectonic blocks of a basin.

Contrarily to the studied sedimentary units, the LTG units and the volcanic units of the Cañadón Asfalto Formation (Geuna *et al.* 2000) preserve the remanence acquired during their formation. To calculate the possible tectonic motions recorded by these units, the method developed by Beck (1976, 1980), Demarest (1983) and Beck *et al.* (1986) was applied (Table 5). To achieve this objective, a palaeomagnetic pole was calculated with the VGPs from both the A and B areas since they belong to the same formation and their directions are equivalent (sites LTG and LTE; see Figs 5 and 6; and Table 5): $N = 11$; Lat.= 77°S; Long.= 73.3°E; $K = 20.2$ and $A95 = 10.4°$.

Also, as explained before, as the normal (negative) and reverse (positive) mean directions from the C area (LTC, see Figs 1 and 2c) are not antipodal, two separate palaeopoles were calculated (Table 5 and Fig. 10). As can be seen in Table 5, when comparing the calculated LTC palaeopoles with the 180 and 170 Ma mean poles of Ruiz Gonzalez *et al*. (2022) and Vaes *et al.* (2023), which correspond to the time of formation of the LTG (Zaffarana & Somoza 2012; Hauser *et al.* 2017; Zaffarana *et al.* 2020), it indicates a lack of rotations about vertical axes. Only the palaeopole obtained from the normal (negative) directions from the C area suggests a possible anticlockwise rotation compared with the 170 Ma mean pole of Vaes *et al*. (2023; Table 5).

However, the VGPs calculated by Geuna *et al.* (2000) from the volcanic units of the Cañadón Asfalto Formation are very close to the ones obtained from the LTG in the C area (LTC; Fig. 10). The main difference is that the VGPs by Geuna *et al.* (2000) are tilt corrected, and those from the C area are *in situ*. These results confirm that the units sampled from the C area correspond effectively to a cinder cone preserved without significant tilting.

On the other hand, the dispersed direction of the VGPs from the volcanic units of the Cañadón Asfalto Formation obtained by Geuna *et al.* (2000) and the LTC VGPs presented in this work is still an unsolved issue. This may represent the record of the EMF during an excursion or reversal since those VGPs correspond to lavas and could correspond to spot readings of the field, due to the instability of the EMF during the Early Jurassic (e.g. Lanza & Zanella 1993; Tarling *et al.* 1999; Vizán & Van Zele 2001).

Recent research indicates that the tectonostratigraphic architecture of the CAB, studied through seismic profiles and fieldwork, discounts a strike-slip tectonic regime (Allard *et al.* 2021a). However, the Jurassic structures within the studied area closely resemble horsetail splay structures, typically linked to transtensional stress regimes (see Fig. 11), but their seismic profiles and the outcrops do not exhibit flower structures (Allard *et al.* 2021a). Additionally, Figari *et al.* (2015) argue that the shape of the basin, divided into depocentres, does not align with the formation of a pull-apart basin, as postulated by Silva Nieto *et al.* (2005). Furthermore, the studied units from the Late Triassic Central Patagonian Batholith in the Gan–Gan domain (Renda *et al.* 2019; domain 2 in Fig. 11a) do not indicate rotations about vertical axes of the blocks (Ruiz González *et al.* 2020).

The interpretation derived from the rotations, which indicate the LTE + LTG pole and the pole calculated by Zaffarana & Somoza (2012) from units of the Lonco Trapial Group and, consequently, the tectonic blocks, whether depocentres or domains (Figari *et al.* 2015; Renda *et al.* 2019), suggests an anticlockwise rotation of 21°–11° (see Table 5). Initially, these findings, in line with the works of Zaffarana & Somoza (2012) and Ruiz González *et al.* (2020), refute the dextral Gastre Fault System proposed by Rapela & Pankhurst (1992), at least since 185 Ma. These block motions also suggest that the stresses that generated the basin were transtensive due to oblique rift extension, as originally proposed by Uliana *et al.* (1989).

Similarly, structural studies to the north of the CAB, in the northern part of the North Patagonian Massif, suggest that regional E-W transfer fault systems led to the segmentation of the rifting (e.g. Benedini & Gregori 2013; Benedini *et al.* 2021). Likewise, in southern Patagonia, in the Deseado Massif, other studies indicate a tectonic evolution in the same direction, with sinistral strike-slip faults (e.g. Reimer *et al.* 1996; Giacosa *et al.* 2010; Fig. 11d). Therefore, when combining the structural evidence described to the north and south of the studied area, the difference in the shear direction of the structures is notable. However, when examining the major structures and block distribution, a resemblance to the San Andreas Fault System can be observed (Fig. 11c). This system is characteristic of strike-slip, and the block structuring in the studied area

would then originate from the Palaeozoic when the stresses between southern and northern Patagonia were transpressive (Renda *et al.* 2019, 2021; Vizán 2023). This igneou–metamorphic belt (Ramos 2008; Renda *et al.* 2019) left a significant structural imprint, which may have served to channel subsequent strain (Renda *et al.* 2019; see Fig. 11d). Thus, during the formation of the CAB, these blocks were reactivated in a direction opposite to the Palaeozoic, generating structures that do not align with those of strike-slip. This can be further confirmed because, in the Central Patagonian Batholith in the Gastre area, field studies, petrology and magnetic fabric indicate that the orientation of structures associated with the Gastre–Sacanana Fault had a sinistral displacement during the emplacement of the granites (Zaffarana *et al.* 2012; Zaffarana *et al.* 2017).

Therefore, it can be inferred that the Lower to Middle Jurassic NNE-SSW extensional regime along Patagonia accommodated the strain along this deformation belt with a sinistral dominant sense, guided by the previous Palaeozoic structures (Zaffarana & Somoza 2012; Renda *et al.* 2019; Ruiz González *et al.* 2022).

4 CONCLUSIONS

In this study, we have successfully identified a remagnetization of the sedimentary units in the CAB, along with the imprinting of a secondary remanence in the volcanic units, around 145 Ma. The resulting pole indicates that, at least since ca. 145 Ma, the strain within the area had no shear component. It also challenges the occurrence of a significant True Polar Wander event during that period (e.g. Kent & Irving 2010). Additionally, the LTG units exhibit a counterclockwise rotation ranging from 21° to 11°. This rotational pattern, consistent with the findings of Zaffarana & Somoza (2012), refutes the Gastre Fault System (Rapela & Pankhurst 1992) since at least ca. 185 Ma. The LTG pole also indicates a shear direction of the structures contrary to those observed to the north and south of Patagonia during the Jurassic suggesting that the inherited Palaeozoic structures from the Central Patagonian Igneous–Metamorphic Belt (e.g. Ramos 2008; Renda *et al.* 2019) may have played a pivotal role in determining the stress direction during the formation of the CAB.

ACKNOWLEDGMENTS

We greatly thank to the owner of the Estancia Los Robles, Juan Eduardo Giacomino Cunningham, for his hospitality and help during these years of work in Paso del Sapo surroundings. Additionally, we would like to thank Eduard Petrovsky (editor), Daniel Pastor Galán and Conall Mac Niocaill (reviewers) for their suggestions and corrections to the manuscript, which have greatly improved the final version. We also thank CONICET (Consejo Nacional de Investigaciones Científicas y Técnicas) and UBA (Universidad de Buenos Aires) for the financial support (PIP 11220120100200CO and UBACyT 20020150100069BA). Part of this work was supported by the multiyear call for the requalification of the Spanish University System for 2021–2023 at the Complutense University of Madrid, funded by the Ministry of Universities with NextGenerationEU funds from the European Union.

SUPPORTING INFORMATION

Supplementary data are available at *GJIRAS* online.

AppendixA.xlsx
AppendixB.xlsx
AppendixC.xlsx
AppendixD.xlsx

Please note: Oxford University Press is not responsible for the content or functionality of any supporting materials supplied by the authors. Any queries (other than missing material) should be directed to the corresponding author for the paper.

DATA AVAILABILITY

Palaeomagnetic raw data are available at: https://osf.io/ukx5v/?view_only=ed6977c7d4d44b6e9963099121fb2bd5.

REFERENCES

Allard, J.O., Foix, N., Paredes, J.M., Giacosa, R.E., Bueti, S.A. & Sánchez, F.M., 2021a. E.2. Estructura y tectónica de las cuenas del Golfo San Jorge y Cañadón Asfalto, in *Geología y Recursos Naturales de la Provincia de Chubut*. Relatorio del XXI Congreso Geológico Argentino, Puerto Madryn, Chubut, 2022, Raul E. Giacosa., pp. 1238–1292, Asociación Geológica Argentina.

Allard, J.O., Paredes, J.M., Foix, N., Giacosa, R.E., Bueti, S.A. & Sánchez, F.M., 2021b. B.5. Estratigrafía de la Cuenca de Cañadón Asfalto, in *Geología y Recursos Naturales de la Provincia de Chubut*. Relatorio del XXI Congreso Geológico Argentino, Puerto Madryn, Chubut, 2022, Raul E. Giacosa., pp. 187–266, Asociación Geológica Argentina.

Ardolino, A.A., Anselmi, G., Giacosa, R.E., Chavez, S.B., Álvarez, M.D., Benítez, J. & Pucheta, A., 2022. Mapa Geológico de la Provincia del Chubut, República Argentina, Escala 1:750.000, Servicio Geológico Minero Argentino. Instituto de Geología y Recursos Minerales. Retrieved from https://repositorio.segemar.gov.ar//handle/308849217/4230.

Barros, M., Gregori, D., Benedini, L., Marcos, P., Strazzere, L., Pivetta, C.P. & Geraldes, M., 2020. Evolution of the Jurassic Comallo volcanic sedimentary complex in the western North Patagonian Massif, Rio Negro province, Argentina, *Int. Geol. Rev.,* **0,** 1–23, doi:10.1080/00206814.2020.1731854.

Beck, M.E., 1976. Discordant paleomagnetic pole positions as evidence of regional shear in the western Cordillera of North America, *Am. J. Sci.,* **276,** 694–712.

Beck, M.E., 1980. Paleomagnetic record of plate-margin tectonic processes along the western edge of North America, *J. geophys. Res.: Solid Earth,* **85,** 7115–7131.

Beck, M.E., Burmester, R.F., Craig, D.E., Gromme', C.S. & Wells, R.E., 1986. Paleomagnetism of middle tertiary volcanic rocks from the Western Cascade Series, northern California, *J. geophys. Res.: Solid Earth,* **91,** 8219–8230.

Benedini, L., *et al.*, 2022. New insights into the Jurassic polyphase strain partition on the patagonian back-arc; constraints from structural analysis of ancient volcanic structures, *Tectonophysics,* **836,** 229430, doi:10.1016/j.tecto.2022.229430.

Benedini, L. & Gregori, D., 2013. Significance of the early jurassic Garamilla formation in the western Nordpatagonian Massif, *J. South Amer. Earth Sci.,* **45,** 259–277.

Benedini, L., Gregori, D., Strazzere, L., Falco, J.I. & Dristas, J.A., 2014. Lower Pliensbachian caldera volcanism in high-obliquity rift systems in the western North Patagonian Massif, Argentina, *J. South Amer. Earth Sci.,* **56,** 1–19.

Benedini, L., *et al.*, 2021. Lower Jurassic felsic diatreme volcanism recognized in central Patagonia as evidence of along-strike rift segmentation, *J. South Amer. Earth Sci.,* **106,** 102705, doi:10.1016/j.jsames.2020.102705.

Biggin, A.J., Steinberger, B., Aubert, J., Suttie, N., Holme, R., Torsvik, T.H., Meer, D.G. van der & van Hinsbergen, D.J.J., 2012. Possible links between long-term geomagnetic variations and whole-mantle convection processes, *Nat. Geosci,* **5,** 526–533.

Bilmes, A., D'Elia, L., Franzese, J.R., Veiga, G.D. & Hernández, M., 2013. Miocene block uplift and basin formation in the Patagonian foreland: the Gastre Basin, Argentina, *Tectonophysics,* **601,** 98–111.

Bouhier, V.E., Franchini, M.B., Caffe, P.J., Maydagán, L., Rapela, C.W. & Paolini, M., 2017. Petrogenesis of volcanic rocks that host the world-class AgPb Navidad District, North Patagonian Massif: comparison with the jurassic Chon Aike Volcanic Province of Patagonia, Argentina, *J. Volc. Geotherm. Res.,* **338,** 101–120.

Bucher, J., *et al.*, 2019. Tectonostratigraphic evolution and timing deformation in the Miocene Paso del Sapo Basin: implications for the Patagonian broken foreland, *J. South Amer. Earth Sci.,* **94,** 102212, doi:10.1016/j.jsames.2019.102212.

Butler, K.L., Horton, B.K., Echaurren, A., Folguera, A. & Fuentes, F., 2020. Cretaceous-cenozoic growth of the Patagonian broken foreland basin, Argentina: chronostratigraphic framework and provenance variations during transitions in Andean subduction dynamics, *J. South Amer. Earth Sci.,* **97,** 102242, doi:10.1016/j.jsames.2019.102242.

Butler, R.F., 1992. *Paleomagnetism: Magnetic Domains to Geologic Terranes,* Blackwell Scientific Publications.

Cabaleri, N. *et al.*, 2010. Estratigrafía, análisis de facies y paleoambientes de la formación cañadón asfalto en el depocentro jurásico cerro Cóndor, provincia del Chubut, *Rev. Asoc. Geol. Argentina,* **66,** 349–367.

Cohen, K.M., Finney, S.C. & Gibbard, P.L.& Fan, and J.-X., 2013. The ICS International Chronostratigraphic Chart, *Episodes J. Int. Geosci.,* **36,** 199–204.

Coira, B., Nullo, F., Proserpio, C. & Ramos, V., 1975. Tectónica de basamento de la región occidental del Macizo Nordpatagónico (provincias de Río Negro y del Chubut), *Rev. Asoc. Geol. Argentina,* **30,** 361–383.

Cúneo, R., Ramezani, J., Scasso, R., Pol, D., Escapa, I., Zavattieri, A.M. & Bowring, S.A., 2013. High-precision U–Pb geochronology and a new chronostratigraphy for the Cañadón Asfalto Basin, Chubut, central Patagonia: implications for terrestrial faunal and floral evolution in Jurassic, *Gondwana Res.,* **24,** 1267–1275.

Dalla Salda, L. & Franzese, J., 1987. Las megaestructuras del macizo y Cordillera Norpatagonica, Argentina y la genesis de las cuencas volcano-sedimentarias Terciarias, *Andean Geol.,* **0,** 3–13, doi:10.5027/andgeoV14n2-a01.

Dalla Salda, L.H., Cingolani, C.A. & Varela, R., 1991. El basamento cristalino de la región norpatagónica de los lagos Gutierrez, Mascardi y Guillelmo, provincia de Río Negro, *Rev. Asoc. Geol. Argentina,* **3–4,** 263–276.

Dalla Salda, L.H., Varela, R., Cingolani, C. & Aragón, E., 1994. The Rio Chico paleozoic crystalline complex and the evolution of Northern Patagonia, *J. South Amer. Earth Sci.,* **7,** 377–386.

Day, R., Fuller, M. & Schmidt, V.A., 1977. Hysteresis properties of titanomagnetites: grain-size and compositional dependence, *Phys. Earth Planet. Inter.,* **13,** 260–267.

Demarest, H.H., 1983. Error analysis for the determination of tectonic rotation from paleomagnetic data, *J. geophys. Res.: Solid Earth,* **88,** 4321–4328.

Di Capua, A. & Scasso, R.A., 2020. Sedimentological and petrographic evolution of a fluvio-lacustrine environment during the onset of volcanism: volcanically-induced forcing of sedimentation and environmental responses, *Sedimentology,* **67,** 1879–1913.

Doubrovine, P.V., Veikkolainen, T., Pesonen, L.J., Piispa, E., Ots, S., Smirnov, A.V., Kulakov, E.V. & Biggin, A.J., 2019. Latitude dependence of geomagnetic paleosecular variation and its relation to the frequency of magnetic reversals: observations from the cretaceous and jurassic, *Geochem. Geophys. Geosyst.,* **20,** 1240–1279.

Dunlop, D.J., 2002. Theory and application of the day plot (Mrs/Ms versus Hcr/Hc) 1. Theoretical curves and tests using titanomagnetite data, *J. geophys. Res.: Solid Earth,* **107,** EPM 4–1-EPM 4-22.

Echaurren, A., Folguera, A., Gianni, G., Orts, D., Tassara, A., Encinas, A., Giménez, M. & Valencia, V.A., 2016. Tectonic evolution of the North Patagonian Andes (41°–44° S) through recognition of syntectonic strata, *Tectonophysics,* **677–678,** 99–114.

Fantasia, A., Föllmi, K.B., Adatte, T., Spangenberg, J.E., Schoene, B., Barker, R.T. & Scasso, R.A., 2021. Late toarcian continental palaeoenvironmental conditions: an example from the Cañadón Asfalto Formation in southern Argentina, *Gondwana Res.,* **89,** 47–65.

Fernández, R.R., Blesa, A., Moreira, P., Echeveste, H., Mykietiuk, K., Palomera, P.A. de & Tessone, M., 2008. Los depósitos de oro y plata vinculados al magmatismo jurásico de la Patagonia: revisión y perspectivas para la exploración, *Rev. Asoc. Geol. Argentina,* **63,** 665–681.

Fernández Lima, J.C. & Latorre, C., 1978. Metalogénesis de la Provincia del Chubut, *Rev. Asoc. Geol. Argentina,* **4,** 355–369.

Figari, E.G. & Courtade, S.F., 1993. Evolución Tectonosedimentaria de la Cuenca d Cañadón Asfalto, Chubut, Argentina, *Actas*, Vol., **I,** pp. 66–77, *Presented at the XII Congreso Geológico Argentino y II Congreso de Exploración de Hidrocarburos,* Asociación Geológica Argentina.

Figari, E.G., Courtade, S.F. & Homovc, J.F., 1992. Estructura de la Cuenca de Cañadón Asfalto, Provincia de Chubut (Inédito), Buenos Aires: Yacimientos Petrolíferos Fiscales.

Figari, E.G., Scasso, R.A., Cúneo, R.N. & Escapa, I., 2015. Estratigrafía y evolución geológica de la Cuenca de Cañadón Asfalto, provincia del Chubut, Argentina, *Latin Am. J. Sedimentol. Basin Anal.,* **22,** 135–169, Asociación Argentina de Sedimentología.

Fisher, R.A., 1953. Dispersion on a sphere, *Proc. R. Soc. Lond. A,* **217,** 295–305.

Foix, N., Allard, J.O., Ferreira, M.L. & Atencio, M., 2020. Spatio-temporal variations in the mesozoic sedimentary record, Golfo San Jorge Basin (Patagonia, Argentina): andean vs. cratonic sources, *J. South Amer. Earth Sci.,* **98,** 102464, doi:10.1016/j.jsames.2019.102464.

Foley, M.L., Putlitz, B., Baumgartner, L.P., Renda, E.M., Ulianov, A., Siron, G. & Chiaradia, M., 2023. Identifying crustal contributions in the Patagonian Chon Aike Silicic large igneous Province, *Contrib. Mineral. Petrol.,* **178,** 80, doi:10.1007/s00410-023-02065-1.

Geuna, S.E., Somoza, R., Vizán, H., Figari, E.G. & Rinaldi, C.A., 2000. Paleomagnetism of jurassic and cretaceous rocks in central Patagonia: a key to constrain the timing of rotations during the breakup of southwestern Gondwana?, *Earth Planet. Sci. Lett.,* **181,** 145–160.

Giacosa, R., Zubia, M., Sánchez, M. & Allard, J., 2010. Meso-cenozoic tectonics of the southern Patagonian foreland: structural evolution and implications for Au–Ag veins in the eastern Deseado Region (Santa Cruz, Argentina), *J. South Amer. Earth Sci.,* **30,** 134–150.

Giacosa, R.E., 2020. Basement control, sedimentary basin inception and early evolution of the mesozoic basins in the Patagonian foreland, *J. South Amer. Earth Sci.,* **97,** 102407, doi:10.1016/j.jsames.2019.102407.

González, S.N., Greco, G.A., González, P.D., Sato, A.M., Llambías, E.J. & Varela, R., 2016. Geochemistry of a Triassic dyke swarm in the North Patagonian Massif, Argentina. Implications for a postorogenic event of the permian Gondwanide orogeny, *J. South Amer. Earth Sci.,* **70,** 69–82.

González, S.N., Greco, G.A., González, P.D., Sato, A.M., Llambías, E.J., Varela, R. & Basei, M.A.S., 2014. Geología, petrografía y edad U-Pb de un enjambre longitudinal NO-SE de diques del Macizo Nordpatagónico oriental, Río Negro, *Rev. Asoc. Geol. Argentina,* **71,** 174–183.

Hauser, N., *et al.*, 2017. U-Pb and Lu-Hf zircon geochronology of the Cañadón Asfalto Basin, Chubut, Argentina: implications for the magmatic evolution in central Patagonia, *J. South Amer. Earth Sci.,* **78,** 190–212.

Heslop, D., Scealy, J.L., Wood, A.T.A., Tauxe, L. & Roberts, A.P., 2023. A bootstrap common mean direction test, *J. geophys. Res.: Solid Earth,* **128,** e2023JB026983, doi:10.1029/2023JB026983

Homovc, J., Figari, E.G. & Courtade, S.F., 1991. Geología de la Cuenca de Cañadón Asfalto, Provincia del Chubut. (Inédito), Buenos Aires: Yacimientos Petrolíferos Fiscales.

Huang, W., *et al.*, 2023. Remagnetization under hydrothermal alteration of south Tibetan paleocene lavas: maghemitization, hematization, and grain size reduction of (Titano)magnetite, *J. geophys. Res.: Solid Earth,* **128,** e2023JB026418, doi:10.1029/2023JB026418.

Iglesia Llanos, M.P., Lanza, R., Riccardi, A.C., Geuna, S., Laurenzi, M.A. & Ruffini, R., 2003. Palaeomagnetic study of the El Quemado complex and Marifil formation, patagonian jurassic igneous province, Argentina, *Geophys. J. Int.,* **154,** 599–617.

Jagadeesh, M.S. & Seehra, M.S., 1981. Thermomagnetic studies of conversion of pyrite and marcasite in different atmospheres (vacuum, H2, He and CO), *J. Phys. D: Appl. Phys.,* **14,** 2153.

Jasonov, P.G., Nourgaliev, D., Burov, B.V. & Heller, F., 1998. A modernized coercivity spectrometer, *Geol. Carpath.,* **49,** 224–225.

Kent, D.V. & Irving, E., 2010. Influence of inclination error in sedimentary rocks on the triassic and jurassic apparent pole wander path for North America and implications for Cordilleran tectonics, *J. geophys. Res.: Solid Earth,* **115,** B10103, doi:10.1029/2009JB007205.

Kirschvink, J.L., 1980. The least-squares line and plane and the analysis of palaeomagnetic data, *Geophys. J. Int.,* **62,** 699–718.

Kulakov, E.V., *et al.*, 2019. Analysis of an updated paleointensity database (QPI-PINT) for 65–200 ma: implications for the long-term history of dipole moment through the mesozoic, *J. geophys. Res.: Solid Earth,* **124,** 9999–10022.

Lanza, R. & Zanella, E., 1993. Palaeomagnetism of the Ferrar dolerite in the northern Prince Albert Mountains (Victoria Land, Antarctica), *Geophys. J. Int.,* **114,** 501–511.

Lesta, P.J., 1968. Estratigrafía de la cuenca del Golfo San Jorge, *3o Jornadas Geológicas Argentinas,* **1,** 251–289.

Lesta, P.J. & Ferello, R., 1972. *Región Extraandina de Chubut y Norte de Santa Cruz. in Simposio de Geología Regional Argentina,* Leanza, A.F., pp. 601–653, Academia Nacional de Ciencias de Córdoba.

Márquez, A.R., Zubía, M.A., Giacosa, R.E., Trevisiol, S.A. & Fernández, M.I., 2016. *Características Geológicas y Metalogenéticas del Depósito Navidad (Ag-Pb-Zn-Cu) Macizo Somún Curá,* Chubut, Argentina. Retrieved from https://repositorio.segemar.gov.ar//handle/308849217/2952.

Martín-Hernández, F., Dekkers, M.J., Bominaar-Silkens, I.M.A. & Maan, J.C., 2008. Magnetic anisotropy behaviour of pyrrhotite as determined by low- and high-field experiments, *Geophys. J. Int.,* **174,** 42–54.

Mazzoni, M.M., Kawashita, K., Harrison, S. & Aragón, E., 1991. Edades radimetricas eocenas. Borde Occidental Del Macizo Norpatagonico, *Rev. Asoc. Geol. Argentina,* **46,** 150–158.

McFadden, P.L., 1990. A new fold test for palaeomagnetic studies, *Geophys. J. Int.,* **103,** 163–169.

McFadden, P.L. & Lowes, F.J., 1981. The discrimination of mean directions drawn from Fisher distributions, *Geophys. J. R. astron. Soc.,* **67,** 19–33.

McFadden, P.L. & McElhinny, M.W., 1990. Classification of the reversal test in palaeomagnetism, *Geophys. J. Int.,* **103,** 725–729.

Moskowitz, B.M., 1981. Methods for estimating Curie temperatures of titanomaghemites from experimentalJs-T data, *Earth planet. Sci. Lett.,* **53,** 84–88.

Nakayama, C., 1973. Sedimentitas pre-Bayocianas en el extremo austral de la Sierra de Taquetrén, Chubut (Argentina), in *Presented at the V Congreso Geológico Argentino*. Asociación Geológica Argentina, pp. 269–277, *Actas*.

Navarro, E.L., Astini, R.A., Belousova, E., Guler, M.V. & Gehrels, G., 2015. Detrital zircon geochronology and provenance of the Chubut Group in the northeast of Patagonia, Argentina, *J. South Amer. Earth Sci.,* **63,** 149–161.

Nicholson, C., Seeber, L., Williams, P. & Sykes, L.R., 1986. Seismic evidence for conjugate slip and block rotation within the San Andreas Fault System, southern California, *Tectonics,* **5,** 629–648.

Nullo, F.E., 1978. *Descripción Geológica de la hoja 41d, Lipetren: Provincia de Río Negro*. Boletin, Dirección Nacional de Minería y Geología. Retrieved from https://repositorio.segemar.gov.ar/handle/308849217/502.

Nullo, F.E., 1983. *Descripción Geológica de la hoja 45c, Pampa de Agnia: Provincia de Chubut*. Boletin, Dirección Nacional de Minería y Geología. Retrieved from https://repositorio.segemar.gov.ar/handle/308849217/420.

Proserpio, C.A., 1987. *Descripción Geológica de la Hoja 44e, Valle General Racedo*. Boletin, Dirección Nacional de Minería y Geología. Retrieved from https://repositorio.segemar.gov.ar//handle/308849217/418.

Ramos, V.A., 2008. Patagonia: a paleozoic continent adrift?, *J. South Amer. Earth Sci.,* **26,** 235–251.

Rapalini, A.E. & Lopez de Luchi, M., 2000. Paleomagnetism and magnetic fabric of middle jurassic dykes from Western Patagonia, Argentina, *Phys. Earth planet. Inter.,* **120,** 11–27.

Rapalini, A.E. & Vilas, J.F., 1991. Preliminary paleomagnetic data from the Sierra Grande formation: tectonic consequences of the first mid-paleozoic paleopoles from Patagonia, *J. South Amer. Earth Sci.,* **4,** 25–41.

Rapela, C.W. & Pankhurst, R.J., 1992. The granites of northern Patagonia and the Gastre Fault System in relation to the break-up of Gondwana, *Geol. Soc. London, Spec. Publ.,* **68,** 209–220.

Reimer, W., Miller, H. & Mehl, H., 1996. Mesozoic and cenozoic palaeostress fields of the South Patagonian Massif deduced from structural and remote sensing data, *Geol. Soc., London, Spec. Publ.,* **108,** 73–85.

Renda, E.M. *et al.*, 2021. Igneous-metamorphic basement of Taquetrén Range, patagonia, Argentina: a key locality for the reconstruction of the paleozoic evolution of patagonia, *J. South Amer. Earth Sci.,* **106,** 103045, doi:10.1016/j.jsames.2020.103045.

Renda, E.M., Alvarez, D., Prezzi, C., Oriolo, S. & Vizán, H., 2019. Inherited basement structures and their influence in foreland evolution: a case study in Central Patagonia, Argentina, *Tectonophysics,* **772,** 228232, doi:10.1016/j.tecto.2019.228232.

Rodríguez-González, A. & Fernández-Turiel, J.L., 2015. Las geoformas volcánicas y su modelado morfométrico con Sistemas de Información Geográfica (SIG), *Enseñanza de las Ciencias de la Tierra,* **23,** 40–40.

Ruiz González, V., Puigdomenech, C.G., Zaffarana, C.B., Vizán, H. & Somoza, R., 2020. Paleomagnetic evidence of the brittle deformation of the Central Patagonian Batholith at Gastre area (Chubut Province, Argentina), *J. South Amer. Earth Sci.,* **98,** 102442, doi:10.1016/j.jsames.2019.102442.

Ruiz González, V., Renda, E.M., Vizán, H., Ganerød, M., Puigdomenech, C.G. & Zaffarana, C.B., 2022. Deformation along the Deseado Massif (Patagonia, Argentina) during the Jurassic Period and its relationship with the Gondwana breakup: paleomagnetic and geochronological constraints, *Tectonophysics,* **834,** 229389, doi:10.1016/j.tecto.2022.229389.

Sangster, A.L., 2001. *Polymetallic Vein Deposits and Occurrences, Central Chubut Province, Argentina*. Recursos Minerales, Vol. 21.

Savignano, E., Mazzoli, S., Arce, M., Franchini, M., Gautheron, C., Paolini, M. & Zattin, M., 2016. (Un)Coupled thrust belt-foreland deformation in the northern Patagonian Andes: new insights from the Esquel-Gastre sector (41°30′–43°, S), *Tectonics,* **35,** 2636–2656.

Silva Nieto, D.G., Márquez, M.J., Ardolino, A.A. & Franchi, M., 2005. *Hoja Geológica 4369-III Paso de Indios,* Servicio Geológico Minero Argentino. Instituto de Geología y Recursos Minerales. Retrieved from https://repositorio.segemar.gov.ar//handle/308849217/165.

Somoza, R. & Zaffarana, C.B., 2008. Mid-cretaceous polar standstill of South America, motion of the Atlantic hotspots and the birth of the Andean cordillera, *Earth planet. Sci. Lett.,* **271,** 267–277.

Stipanicic, P.N., Rodrigo, F., Baulies, O.L. & Martínez, C.G., 1968. Las formaciones presenonianas en el denominado Macizo Nordpatagónico y regiones adyacentes, *Rev. Asoc. Geol. Argentina,* **23,** 67–98.

Tarling, D.H., Iorio, M. & D'Argenio, B., 1999. Geomagnetic long-term secular variations in Italian lower cretaceous shallow-water carbonates, *Geophys. J. Int.,* **137,** 713–722.

Uliana, M.A., Biddle, K.T. & Cerdan, J., 1989. Mesozoic extension and the formation of Argentine sedimentary basins, in A.J., Tankard, & Balkwill, H.R., eds, *Extensional Tectonics and Stratigraphy of the North Atlantic Margins,* Vol., **46,** American Association of Petroleum Geologists, doi:10.1306/M46497C39.

Vaes, B., *et al.*, 2023. A global apparent polar wander path for the last 320 ma calculated from site-level paleomagnetic data, *Earth Sci. Rev.,* **245,** 104547, doi:10.1016/j.earscirev.2023.104547.

Van der Voo, R., 1990. The reliability of paleomagnetic data, *Tectonophysics,* **184,** 1–9.

Vilas, J.F.A., 1974. Palaeomagnetism of some igneous rocks of the middle jurassic Chon-Aike Formation from Estancia La Reconquista, Province of Santa Cruz, Argentina, *Geophys. J. Int.,* **39,** 511–522.

Vizán, H., 1998. Paleomagnetism of the lower jurassic Lepá and Osta Arena formations, Argentine Patagonia, *J. South Amer. Earth Sci.,* **11,** 333–350.

Vizán, H., 2023. The Paleozoic Central patagonian Igneous Metamorphic Belt: its geodynamic and tectonic interpretation based on paleogeographic reconstructions, *Int. J. Earth Sci. (Geol Rundsch),* **112,** 2081–2096.

Vizán, H. & Van Zele, A.M., 2001. Analysis of the early Jurassic geomagnetic data recorded at the Breggia Gorge (Ticino, Switzerland), *Phys. Earth planet. Inter.,* **125,** 19–29.

Volkheimer, W., Gallego, O.F., Cabaleri, N.G., Armella, C., Narváez, P.L., Silva Nieto, D.G. & Páez, M.A., 2009. Stratigraphy, palynology, and conchostracans of a lower cretaceous sequence at the Cañadón Calcáreo locality, extra-andean central Patagonia: age and palaeoenvironmental significance, *Cretaceous Res.,* **30,** 270–282.

Wood, C.A., 1980. Morphometric evolution of cinder cones, *J. Volc. Geotherm. Res.,* **7,** 387–413.

Zaffarana, C. *et al.*, 2018. Geochemical signature and reservoir conditions of early Jurassic calc-alkaline volcanic rocks from Lonco Trapial Formation, Central Patagonia, *J. South Amer. Earth Sci.,* **88,** 415–445.

Zaffarana, C.B. *et al.*, 2020. Petrogenetic study of the Lonco Trapial volcanism and its comparison with the early-Middle Jurassic magmatic units from northern Patagonia, *J. South Amer. Earth Sci.,* **101,** 102624, doi:10.1016/j.jsames.2020.102624.

Zaffarana, C.B., López de luchi, M.G., Somoza, R., Mercader, R., Giacosa, R. & Martino, R.D., 2010. Anisotropy of magnetic susceptibility study in two classical localities of the Gastre Fault System, central Patagonia, *J. South Amer. Earth Sci.,* **30,** 151–166.

Zaffarana, C.B., Montenegro, T. & Somoza, R., 2012. The host rock of The Central patagonian batholith In gastre: further insights on The late triassic to early jurassic deformation In The region, *Rev. Asoc. Geol. Argentina,* **69,** 106–126.

Zaffarana, C.B. & Somoza, R., 2012. Palaeomagnetism and 40Ar/39Ar dating from lower jurassic rocks in Gastre, central Patagonia: further data to explore tectonomagmatic events associated with the break-up of Gondwana, *J. Geol. Soc.,* **169,** 371–379.

Zaffarana, C.B., Somoza, R., Orts, D.L., Mercader, R., Boltshauser, B., Ruiz González, V. & Puigdomenech, C., 2017. Internal structure of the late triassic Central patagonian batholith at Gastre, southern Argentina: implications for pluton emplacement and the Gastre fault system, *Geosphere,* **13,** 1973–1992.

Zijderveld, J.D.A., 1967. A. C. demagnetization of rocks: analysis of results, in *Developments in Solid Earth Geophysics* Methods in Palaeomagnetism, Vol., **3,** pp. 254–286, eds. Collinson, D.W., Creer, K.M. & Runcorn, S.K., Elsevier.